Structural Characterization of an Analog of the Major Rate-Determining Disulfide Folding Intermediate of Bovine Pancreatic Ribonuclease A†

John H. Laity,‡,|| Cathy C. Lester,‡ Sakurako Shimotakahara,‡,§ Diane E. Zimmerman,§ Gaetano T. Montelione,*,§ and Harold A. Scheraga*,‡

Baker Laboratory of Chemistry, Cornell University, Ithaca, New York 14853-1301, and Center for Advanced Biotechnology and Medicine and Department of Molecular Biology and Biochemistry, Rutgers University, Piscataway, New Jersey 08854-5638

Received April 15, 1997; Revised Manuscript Received July 30, 1997⊗

ABSTRACT: The major rate-determining step in the oxidative regeneration of bovine pancreatic ribonuclease A (RNase A) proceeds through des-[40−95] RNase A, a three-disulfide intermediate lacking the Cys40−Cys95 disulfide bond. An analog of this intermediate, [C40A, C95A] RNase A, has been characterized in terms of regular backbone structure and thermodynamic stability at pH 4.6. Nearly complete backbone ^{1}H, ^{15}N, and ^{13}C resonances, and most $^{13}C^{\beta}$ side-chain resonances have been assigned for the mutant RNase A using triple-resonance NMR data and a computer program, AUTOASSIGN, for automated analysis of resonance assignments. Comparisons of chemical shift data, $^{3}J(^{1}H^{N}-^{1}H^{\alpha})$ coupling constants, and NOE data for the mutant and wild-type proteins reveal that the overall chain folds of the two proteins are very similar, with localized structural perturbations in the regions spatially adjacent to the mutation sites in [C40A, C95A] RNase A. More significantly, $^{1}H/^{2}H$ amide exchange and thermodynamic data reveal a global destabilization of the mutant protein characterized by a significant difference in the midpoint of the thermal transition curves (ΔT_m of 21.8 °C) and a significant increase in the slowest exchanging backbone amide $^{1}H/^{2}H$ exchange rates ($10^{2}-10^{6}$-fold faster in the hydrophobic core of [C40A, C95 A] RNase A). Comparisons of the entropy $\Delta S°(T)$ and enthalpy $\Delta H°(T)$ of unfolding between wild-type and [C40A, C95A] RNase A reveal that some of the global destabilization of the mutant protein arises from entropic and enthalpic changes in the folded state. Implications of these observations for understanding the role of des-[40−95] in the folding pathway of RNase A are discussed.

Protein folding proceeds through a series of intermediates that define the pathway from the unfolded polypeptide to the native structure. The nature of the interactions responsible for this process is determined solely by the amino acid sequence of the protein (Anfinsen, 1973). For many proteins, disulfide bond formation is an essential component of the folding process and subsequent stabilization of the folded structure (Creighton, 1974, 1977a,b, 1988; Thornton, 1981; Richardson, 1981; Konishi et al., 1981, 1982a−c; Creighton & Goldenberg, 1984; Scheraga et al., 1987; Altmann & Scheraga, 1990; Weissman & Kim, 1991, 1992a,b, 1993, 1995; Rothwarf & Scheraga, 1991, 1993a−d; Rothwarf et al., 1995; Doig & Williams, 1991; Goldenberg, 1992; Dadlez & Kim, 1996). One disulfide-containing protein in particular, bovine pancreatic ribonuclease A (RNase A),[1] has been studied extensively in terms of its folding and unfolding pathways (Hantgen et al., 1974; Ahmed et al., 1975; Creighton, 1977a,b; Wearne & Creighton, 1988; Konishi et al., 1981, 1982a−c; Rothwarf & Scheraga, 1991, 1993a−d; Rothwarf et al., 1995; Li et al., 1995). RNase A is a 124-residue protein containing four native disulfide bonds (Cys26−Cys84, Cys40−Cys95, Cys58−Cys110, and Cys65−Cys72) that folds through multiple pathways, with the rate-determining steps in the major and minor populated pathways involving the formation of the three-disulfide species des-[40−95][1] and des-[65−72],[1] respectively (Rothwarf et al., 1995). Recently, Li et al. (1995) observed the same two three-disulfide *folding intermediates* of RNase A as intermediates in parallel *reduction* pathways, with each intermediate possessing a structurally distinct transition state. Using the kinetic applicability of reduction rate constants to regeneration studies and vice versa, the authors suggest that the regeneration and reduction pathways are the same in RNase A (Li et al., 1995).

† This work was supported by grants from the National Institutes of Health (GM-24893 to H.A.S. and GM-47014 to G.T.M.), the National Foundation for Cancer Research (to H.A.S.), and the National Science Foundation (MCB-9407569 to G.T.M). J.H.L. and S.S. were NIH trainees, and C.C.L. was an NIH Postdoctoral Fellow at Cornell University.

* Address correspondence to H.A.S. (phone, 607-255-4034; Fax, 607-254-4700; e-mail, has5@cornell.edu) or G.T.M. (phone, 908-235-5321; Fax, 908-235-4850; e-mail, guy@nmrlab.cabm.rutgers.edu).

‡ Cornell University.

|| Present address: Department of Molecular Biology (MB-2), The Scripps Research Institute, La Jolla, CA 92037.

§ Rutgers University.

⊗ Abstract published in *Advance ACS Abstracts,* October 1, 1997.

[1] Abbreviations: RNase A, bovine pancreatic ribonuclease A; [C40A, C95A] RNase A, three-disulfide mutant of RNase A with replacement of cysteines 40 and 95 by alanine; [C40S, C95S] RNase A, three-disulfide mutant of RNase A with replacement of cysteines 40 and 95 by serine; des-[40−95] and des-[65−72], three-disulfide species of RNase A with native disulfide bonds Cys26−Cys84 and Cys58−Cys110 but lacking either the Cys40−Cys95 (des-[40−95]) or the Cys65−Cys72 (des-[65−72]) disulfide bond; BPTI, bovine pancreatic trypsin inhibitor; cCMP, cyclic cytidine 2′,3′-monophosphate; 2D, two dimensional; 3D, three dimensional; GSs, generic amino acid spin systems with no site-specific assignment; CFIS, chain folding initiation site; MALDI-TOF, matrix-assisted laser desorption ion−time of flight; $^{1}H/^{2}H$ exchange, amide proton hydrogen/deuterium exchange; HSQC, heteronuclear single-quantum coherence; NOESY, nuclear Overhauser effect spectroscopy; TOCSY, total correlated spectroscopy; pH*, pH meter reading of an $^{2}H_2O$ solution not corrected for the deuterium isotope effect; PFG, pulsed-field gradient; $\Delta\delta$, difference in chemical shift in parts per million (ppm); $\Delta\delta C^{\alpha}$, difference in α-carbon chemical shift in parts per million (ppm); ΔJ, difference in $^{3}J(H^{N}-H^{\alpha})$ coupling constants in hertz (Hz).

S0006-2960(97)00878-7 CCC: $14.00

These kinetic studies have specified the crucial intermediates in the regeneration and reduction pathways of RNase A. However, identifying the specific interresidue interactions responsible for the conformational folding events that produce these intermediates, and ultimately the native protein, remains one of the most fundamental and largely unanswered questions in protein folding (Kim & Baldwin, 1990). Recent advances in nuclear magnetic resonance (NMR) spectroscopy, primarily through the use of triple-resonance experiments involving uniformly ^{15}N- and ^{13}C-enriched proteins, have provided new insights into the structure, stability, and conformational dynamics of proteins (Wüthrich, 1989; Clore & Gronenborn, 1991; Bax & Grzesiek, 1993; Kay, 1995; Zimmerman & Montelione, 1995; Palmer et al., 1996). NMR methods have been utilized to characterize the solution structures of the major folding intermediates in BPTI[1] (Naderi et al., 1991; van Mierlo et al., 1991, 1993; Hurle et al., 1992; Darby et al., 1992; Staley & Kim, 1992) and, more recently, of both thiol-blocked and [C65S, C72S][1] analogs of the des-[65−72] rate-determining intermediate of RNase A (Talluri et al., 1994; Shimotakahara et al., 1997). These NMR studies of the des-[65−72] analogs indicate that there are two adjacent regions of small localized structural perturbations, the first being the loop region where the Cys65 and Cys72 residues are located in the wild-type protein and the second the hydrophobic core of the protein. One of the most significant observations from these studies of des-[65−72], however, is that the small loop formed by the Cys65−Cys72 disulfide bond contributes significantly to stabilizing the β-sheet of the hydrophobic core in the wild-type protein.

Destabilization of des-[65−72], indicated by NMR evidence, is corroborated by the significant difference in the midpoints of the thermal transitions ($\Delta T_m \sim 17$ °C) between wild-type and [C65S, C72S] RNase A at pH 6.4 (Laity et al., 1993) and similar differences in the T_m's of both thiol-blocked and [C65S, C72S] RNase A analogs at pH 4.6 (Talluri et al., 1994; Shimotakahara et al., 1997). The corresponding entropies [$\Delta S°(T_m)$] and enthalpies [$\Delta H°(T_m)$] of unfolding, which have been determined for both analogs, provide further evidence for global stabilization of the native chain fold upon formation of the Cys65−Cys72 cross-link in wild-type RNase A (Talluri et al., 1994; Shimotakahara et al., 1997). Similarly, large increases in all observable amide ^{1}H/^{2}H exchange[1] rates in [C65S, C72S] RNase A relative to the wild-type protein at pH* [1] 4.6 also show the global stabilizing effect of the Cys65−Cys72 disulfide bond in wild-type RNase A.

The peptide bonds preceding proline residues are unique in proteins in that they can exist in one of two isomeric states, cis or trans, in the native structure, whereas other peptide bonds exist almost exclusively in the trans conformation. Wild-type RNase A has four proline residues at positions 42, 93, 114, and 117. In the crystal structure of wild-type RNase A, the Lys41−Pro42 and Val116−Pro117 peptide bonds are in the trans conformation, while the Tyr92−Pro93 and Asn113−Pro114 peptide bonds are in the cis conformation (Wlodawer, 1980). Houry et al. (1994) have shown that the fastest disulfide-intact folding phase of RNase A (U_{vf}) involves X−Pro isomers that are all in the same isomeric states as those present in the native protein structure. Moreover, the region encompassing the Tyr92−Pro93 peptide bond, which forms a type VI β-turn, is believed to form one of the local chain folding initiation sites (CFIS[1]) in RNase A (Matheson & Scheraga, 1978; Némethy & Scheraga, 1979; Montelione et al., 1984; Oka et al., 1984; Montelione & Scheraga, 1989). Identification and subsequent characterization of CFIS's, which are believed to form before the major conformational folding events take place in a protein, are important areas of active investigation in the field of protein folding (Némethy & Scheraga, 1979; Wright et al., 1988; Montelione & Scheraga, 1989; Udgaonkar & Baldwin, 1990; Buckler et al., 1995; Dodge & Scheraga, 1996; Xu et al., 1996; Freund et al., 1996). As a result of the deletion of the native cystine Cys40−Cys95 cross-link in RNase A, the region encompassing the X−Pro93 type VI β-turn is likely to exhibit increased flexibility which would allow it to explore more conformational space than that which is available to the wild-type protein. Accordingly, characterization of the isomeric state of the X−Pro93 peptide bond in a mutant form of RNase A which lacks the Cys40−Cys95 disulfide bond will provide further insight into the long-range effects responsible for stabilizing the cis X−Pro93 conformation in this proposed CFIS region of wild-type RNase A.

The primary focus in this study is to characterize an analog of des-[40−95], the *major* rate-determining oxidative folding intermediate of RNase A, by identifying the location and magnitude of conformational distortions that result from the removal of the Cys40−Cys95 disulfide bond. For this purpose, we have produced a uniformly ^{15}N,^{13}C-labeled mutant analog of des-[40−95] RNase A in which the native Cys40 and Cys95 residues have been replaced by alanine residues ([C40A, C95A] RNase A[1]). We have determined nearly complete backbone ^{1}H, ^{15}N, ^{13}C, and most side-chain $^{13}C^{\beta}$ resonance assignments for this mutant analog of des-[40−95] RNase A. These assignments, coupled with the corresponding assignments for the wild-type protein (Shimotakahara et al., 1997), serve as the basis for detailed investigations of the differences in structure, stability, and conformational flexibility between the mutant and wild-type proteins. Comparisons between chemical shift, $^3J(H^N-H^{\alpha})$ scalar coupling constants, NOE, and amide ^{1}H/^{2}H exchange data for wild-type (Shimotakahara et al., 1997) and [C40A, C95A] RNase A provide detailed information about these structural and dynamic differences. To expedite the resonance assignment procedure, an expert system, AUTOASSIGN (Zimmerman et al., 1994, 1997), was employed for automated analysis of the triple-resonance NMR data.

Results of NMR and thermodynamic data obtained from [C40A, C95A] RNase A reveal significant localized structural alterations in the two regions where the Cys40 and Cys95 residues are present in the wild-type protein. Despite these local perturbations in structure, chemical shift data are presented which indicate that the Tyr92−Pro93 peptide bond of the major conformer of [C40A, C95A] RNase A is predominantly in the cis peptide bond conformation. Furthermore, these data demonstrate clearly that the Cys40−Cys95 cross-link in native RNase A affords a substantial stabilization of the overall global chain fold of the protein. This stabilizing influence of the Cys40−Cys95 disulfide bond is even *more pronounced* than that which is observed for the Cys65−Cys72 disulfide bond. Moreover, structural and thermodynamic comparisons presented here of analogs of the rate-determining folding intermediates des-[40−95] and des-[65−72] corroborate the existence of conformationally

distinct transition states for the two parallel regeneration/reduction pathways of wild-type RNase A.

MATERIALS AND METHODS

Construction of a DNA Expression Vector for Mutant RNase A. Mutant RNase A for thermal transitions and activity measurements was expressed using the pSJII[C40A, C95A] and pSJII[C40S, C95S] DNA vectors (Laity et al., 1993). Uniformly ^{15}N- and ^{15}N,^{13}C-enriched [C40A, C95A] RNase A and unlabeled [C40A, C95A] and [C40S, C95S][1] RNase A were produced using the DNA expression vectors pRM[C40A, C95A] and pRM[C40S, C95S]. Similarly, uniformly ^{15}N-enriched wild-type RNase A was produced using the DNA expression vector PXBR-2 (delCardayré et al., 1995). The construction of the mutant RNase A DNA vectors was based on the corresponding wild-type vector pXBR-2. The pRM[C40A, C95A] and pRM[C40S, C95S] DNA constructs were made by subcloning the mutated RNase A gene from pSJII[C40A, C95A] and pSJII[C40S, C95S], respectively (Laity et al., 1993), into a pET22b DNA vector (Novagen). The original synthetic wild-type gene from which the mutant RNase A DNA vectors were constructed was a gift from the Genex Corp. The mutant RNase A genes were inserted into the multiple cloning site of the pET22b DNA vector between the *Msc*I restriction site on the 5′ end of the gene and the *Hind*III restriction site on the 3′ end of the gene. The necessary *Msc*I restriction sites at the beginning of the mutant RNase A genes in pSJII[C40A, C95A] and pSJII[C40S, C95S] were created using polymerase chain reaction (PCR) methodology (Perkin-Elmer Gene Amp PCR System 2400). All other DNA restriction sites used in the cloning process were already present on the respective DNA vectors. The sequences of all DNA expression vectors were confirmed by DNA sequencing at the Cornell Biotechnology Analytical Facility. All oligonucleotides used for PCR were synthesized at the same facility.

Protein Expression. The protein expression system described by Laity et al. (1993) was used to produce all unenriched mutant proteins using *Escherichia coli* strain HMS174(DE3)plys S as the bacterial host. Expression of uniformly ^{15}N-enriched mutant and wild-type RNase A and ^{15}N,^{13}C-enriched [C40A, C95A] RNase A is described here. The DNA plasmid containing the mutant (pRM[C40A, C95A]) or wild-type (PXBR-2) RNase A gene was transformed into competent *E. coli* BL21(DE3) cells and grown overnight at 37 °C on an agar plate (Difco Plate Count Agar) containing 200 μg/mL ampicillin. A single colony of cells containing the mutant RNase A DNA vector was grown in 15−25 mL of liquid broth (LB) media containing 200 μg/mL ampicillin at 37 °C with constant agitation on a gyrotary shaker at 225 rpm. When the optical density at 610 nm (OD_{610}) of the cell culture reached 0.7−0.8, it was centrifuged at 2500 rpm for 10 min, and the supernatant was decanted. The cell pellet was used to inoculate 1 L of MJ minimal media (Jansson et al., 1996) containing 50 μg/mL ampicillin. The 2.5 g/L $(^{15}NH_4)_2SO_4$ and, for ^{15}N,^{13}C-enriched protein, the 2.0 g/L [U-^{13}C]glucose were the only metabolic sources of nitrogen and carbon, respectively. The culture was incubated under the same conditions as the inoculate until the OD_{610} reached 0.7−0.9. Then, to induce protein expression, 1 mL of a 0.5 M solution of isopropyl β-D-thiogalactopyranoside (IPTG) in H_2O was added to the cell culture, which was subsequently grown for 3−8 h at 37 °C. The expressed protein, linked at the N-terminus of the mutant RNase A to the leader peptide PelB, was subsequently processed *in vivo* to produce homogeneous [C40A, C95A] RNase A. All of the mutant RNase A recovered from the *E. coli* cells was in the form of insoluble inclusion bodies.

Protein Isolation and Purification. All of the unenriched mutant RNase A used for thermal denaturation studies and activity measurements was recovered from the *E. coli* and purified as described previously (Laity et al., 1993). *E. coli* cells containing isotopically enriched mutant or wild-type RNase A expressed from either the pRM[C40A, C95A] or the PXBR-2 DNA clones were harvested by centrifugation at 7000 rpm with a Beckman JA-10 rotor for 20 min. The cell pellet was then resuspended in 100 mL of lysis buffer [25 mM Tris-HCl/5 mM EDTA/0.5% (v/v) Triton X-100, pH 8.0] and immediately frozen at −70 °C to lyse the cells completely. The solution was thawed to room temperature and sonicated (Ultrasonics cell sonicator) to extricate inclusion bodies from the cell membranes. Sonication was carried on for 3 min, using 1 s pulses with a 2 s delay between each pulse to avoid excessive sample heating. The cell lysate was centrifuged for 1 h at 7000 rpm, and the resulting insoluble pellet was dissolved in 20−30 mL, depending on the estimated yield of the expressed inclusion bodies, of 7 M Gdn-HCl/25 mM Tris-HCl/5 mM EDTA/0.3 M Na_2SO_3, pH 8.0. The solubilized inclusion body solution was then centrifuged at 15 000 rpm for 15 min to remove any insoluble material. The supernatant was next sulfonated by the procedure of Thannhauser and Scheraga (1985). The reversibly S-sulfonated mutant RNase A was then dialyzed with at least two buffer changes in a 40-fold volume of 50 mM formic acid/3 M urea, pH 4.0 at 4 °C. Most of the nonrecombinant cellular proteins dissolved during the dialysis, leaving the supernatant to contain ∼90% of the S-sulfonated mutant RNase A, as judged by 12% SDS−PAGE. The dialysate was then centrifuged at 15 000 rpm for 15 min, and the supernatant was exchanged into refolding buffer (0.1 M Tris-HCl/3 mM EDTA, pH 8.2) using a preequilibrated 45 cm × 2.5 cm column (Ace Glass) packed with Sepharose G-25M resin (Pharmacia). The solution was diluted with refolding buffer to a protein concentration of 0.2−0.4 mg/mL, as judged by UV spectroscopy using the extinction coefficient of S-sulfonated wild-type RNase A at 275 nm of 8500 M^{-1} cm^{-1} (Thannhauser & Scheraga, 1985).

Oxidative regeneration of mutant RNase A was initiated by the addition at 4 °C of a 1:10 volume of 10 mM/20 mM (oxidized/reduced) glutathione (Boehringer Manneheim) in refolding buffer. The solution was incubated at 4 °C for 48 h, and then concentrated to 2−6 mL (5−10 mg of mutant RNase A/mL), depending on the estimated yield of regenerated protein, using an Amicon concentrator with a YM-3 membrane. Glacial acetic acid was added to the protein solution to a final concentration of 100 mM, and the solution was centrifuged at 15 000 rpm to remove any precipitated protein. The supernatant was filtered through a 0.2 μm disk membrane (Gelman) and purified by ion-exchange HPLC using a preparative Rainin Hydropore column (5 cm diameter) and a linear NaCl gradient of 0−15% in 40 min (8 mL/min flow rate). The purified protein was concentrated and exchanged into 100 mM acetic acid using a preequilibrated 1 cm × 20 cm Sepharose G-25M column. HCl (1 M) was added to a final concentration of 2−3 mM. The

protein solution was then frozen and lyophilized. Addition of HCl to the mutant RNase A solution after desalting into acetic acid results in the preferential occurrence of Cl^- as the counterion in lyophilized RNase A which is both advantageous in, and confirmed by, ^{1}H NMR experiments. The one-dimensional ^{1}H NMR spectrum of [C40A, C95A] RNase A, with HCl added prior to lyophilization, shows no acetate peak. In contrast, the ^{1}H NMR spectrum of the same protein lyophilized *without* prior addition of HCl shows a large acetate peak in the protein aliphatic region (J. H. Laity, D. M. Rothwarf, and H. A. Scheraga, unpublished results). The yield of purified mutant and wild-type RNase A in MJ minimal media was 4−8 mg/L.

Nonrecombinant RNase A type I−A (Sigma) used for thermodynamic and enzymatic measurements was purified further using a preequilibrated S-Sepharose ion-exchange column as described by Rothwarf and Scheraga (1993a).

Protein Characterization. Molecular weights of all mutant RNase A protein samples were determined using matrix-assisted laser desorption ionization−time of flight mass spectrometry (MALDI-TOF MS[1]). This analysis was especially important for confirming uniform isotopic enrichment (∼99%) of the mutant and wild-type RNase A NMR samples. Correct N-terminal processing of the Pel B−mutant RNase A fusion protein was confirmed by N-terminal protein sequencing. All recombinant and nonrecombinant RNase A samples were determined to be >99% free of deamidated protein (Thannhauser & Scheraga, 1985) or other impurities as judged by amino acid analysis, by analytical ion-exchange chromatography using a Rainin Hydropore analytical HPLC column, and by capillary gel electrophoresis (CE[1]). All uniformly ^{15}N-enriched mutant and wild-type and ^{15}N,^{13}C-enriched [C40A, C95A] RNase A samples used in the NMR experiments were analyzed for chemical degradation by analytical HPLC and CE *after* the NMR experiments were completed to determine if any degradation occurred during the course of NMR data collection. MALDI-TOF MS, N-terminal protein sequencing, amino acid analysis, and CE were carried out at the Cornell Biotechnology Analytical Facility.

Thermal Transitions. The method used to monitor reversible thermal denaturation was that of Laity et al. (1993). All protein concentrations were kept low (∼12 μM) to avoid aggregation during the protein denaturation/renaturation process. Absorbance measurements were made using 10 cm path-length quartz cells (Hellma). All thermal transition curves were determined in 100 mM sodium acetate, pH 4.60 ± 0.05.

Enzymatic Activity. Mutant and nonrecombinant wild-type RNase A activity measurements were made in 50 mM Tris-HCl/0.1 M NaCl, pH 5.00 at 22 °C, using cyclic cytidine 2′,3′-monophosphate (cCMP[1]) as a substrate (Crook et al., 1960).

NMR Sample Preparation. Uniformly ^{15}N-enriched mutant and wild-type and uniformly ^{15}N,^{13}C-enriched [C40A, C95A] RNase A samples were prepared by dissolving the lyophilized protein in 90%/10% ($^1H_2O/^2H_2O$) at pH* 4.60 ± 0.05. All NMR measurements were made using 5 mm susceptibility-matched Shigemi NMR tubes at 20 °C. The uniformly ^{15}N,^{13}C-enriched [C40A, C95A] RNase A sample concentration was 2.4 mM, the ^{15}N-enriched [C40A, C95A] RNase A sample concentrations ranged from 3.5 to 4.5 mM, and the ^{15}N-enriched wild-type RNase A sample concentration was 3.0 mM.

NMR Spectroscopy. All triple-resonance NMR spectra were recorded on a Varian Unity 500 NMR spectrometer system (at CABM, Rutgers) equipped with three full channels and modified to provide a computer-controlled fourth synthesizer. All homonuclear and heteronuclear 2D[1] as well as 3D[1] ^{15}N-edited experiments were recorded on a Varian Unity 500 NMR spectrometer (at Cornell) equipped with three full channels. The 3D ^{13}C-edited NOESY[1] spectrum was recorded on a Varian Unity Plus 600 NMR spectrometer system at Cornell. Phase-sensitive data were acquired either by using the States−TPPI method (Marion et al., 1989) or by combining n- and p-spectra (Nagayama, 1986; Kay et al., 1992) selected with pulsed-field gradients (PFG's).[1]

Pulsed-field gradient triple-resonance experiments were carried out on uniformly ^{15}N,^{13}C-enriched [C40A, C95A] RNase A. A detailed description of these triple-resonance NMR pulse sequences has been presented elsewhere (Shimotakahara et al., 1997). For all triple-resonance experiments, the spectral width was 2500 Hz in the nitrogen dimension (t_2) and 6900 Hz in the direct proton dimension (t_3), with the proton carrier set to the water frequency to reduce the amplitude of spurious water echoes.

3D PFG-HNCO data [based on Muhandiram and Kay (1994)] were acquired using 40 × 40 × 1024 complex points in the t_1, t_2, and t_3 dimensions with four scans per increment. The spectral width in the carbon (t_1) dimension was 2000 Hz. Coherence transfer delays were tuned to $\tau_a = 2.4$ ms and $\tau_b = 13$ ms. The constant time evolution period was tuned to $\tau_f = 13$ ms.

3D PFG-HN(CA)CO data [based on Clubb et al. (1992)] were acquired using 40 × 45 × 1024 complex points in the t_1, t_2, and t_3 dimensions with 24 scans per increment. The spectral width in the carbon (t_1) dimension was 2000 Hz. Coherence transfer delays were tuned to $\tau_a = 2.3$ ms and $\tau_b = 3.0$ ms. The constant time evolution period was tuned to $\tau_c = 10$ ms.

3D PFG-HNCA data [based on Muhandiram and Kay (1994)] were acquired using 40 × 40 × 1024 complex points in the t_1, t_2, and t_3 dimensions with eight scans per increment. The spectral width in the carbon (t_1) dimension was 6100 Hz. Coherence transfer delays were tuned to $\tau_a = 2.4$ ms and $\tau_b = 11$ ms. The constant time evolution period was tuned to $\tau_f = 11$ ms.

3D PFG-C(CO)NH data (Boucher et al., 1992; Feng et al., 1996) were acquired using 40 × 45 × 1024 complex points in the t_1, t_2, and t_3 dimensions with 16 scans per increment. The spectral width in the carbon (t_1) dimension was 6100 Hz. Coherence transfer delays were tuned to $\tau_a = 1.5$ ms, $\tau_{a-foc} = 2.4$ ms, $\tau_b = 4.2$ ms, $\tau_c = 2.4$ ms, and $\tau_d = 14.0$ ms. The constant time evolution periods were tuned to $T_c = 3.3$ ms and $T_n = 14.0$ ms.

Data for both 3D PFG-H(C)(CO)NH (Boucher et al., 1992; Feng et al., 1996) and 3D PFG-H(C)NH (Montelione & Wagner, 1989; Feng et al., 1996) were acquired using 40 × 45 × 1024 complex points in the t_1, t_2, and t_3 dimensions with 16 scans per increment. Both experiments were carried out with a spectral width in the aliphatic proton (t_1) dimension of 3000 Hz, and coherence transfer delays were tuned to $\tau_a = 1.5$ ms, $\tau_{a-foc} = 2.4$ ms, $\tau_b = 4.2$ ms, $\tau_c = 2.4$ ms, and $\tau_d = 14.0$ ms. The constant time evolution periods were tuned to $T_c = 3.3$ ms and $T_n = 14.0$ ms.

Data for both 3D PFG-CBCA(CO)NH (Grzesiek & Bax, 1992a; Rios et al., 1996) and 3D PFG-CBCANH (Grzesiek & Bax, 1992b; Rios et al., 1996) were acquired using 40 x 45 × 1024 complex points in the t_1, t_2, and t_3 dimensions with 16 scans per increment. Both experiments were carried out with a spectral width in the carbon (t_1) dimension of 10000 Hz, and coherence transfer delays were tuned to $\tau_a = 1.5$ ms, $\tau_{a-foc} = 2.4$ ms, $\tau_b = 4.4$ ms, $\tau_c = 2.4$ ms, and $\tau_d = 12.0$ ms, and $\tau_e = 4.1$ ms. The constant time evolution periods were tuned to $T_c = 3.3$ ms and $T_n = 13$ ms.

The 2D NOESY spectrum (Jeener et al., 1979; Kumar et al., 1980; Macura & Ernst, 1980) was recorded using 512 complex points and a spectral width of 6900 Hz in the t_1 dimension and 2048 complex points and a spectral width of 6900 in the t_2 dimension. 3D PFG ^{15}N-edited NOESY (Macura & Ernst, 1980) and 3D PFG ^{15}N-edited TOCSY experiments (Braunschweiler & Ernst, 1983; Bax & Davis, 1985) were based on the 3D ^{15}N-edited NOESY experiment of Zuiderweg and Fesik (1989), with modifications to provide coherence transfer by TOCSY in the latter experiment. Both pulse sequences [described in Shimitakahara et al. (1997)] were modified to provide heteronuclear coherence selection for water suppression (Hurd & John, 1991) and were carried out using 150 × 64 × 1024 complex data points in the t_1, t_2, and t_3 dimensions and four scans per increment. The spectral widths for both experiments were 6500 Hz in t_1, 2500 Hz in t_2, and 3500 Hz in t_3, with the offset switched to the center of the amide region prior to acquisition. The NOESY mixing times were all 80 ms and the TOCSY mixing time was 47.8 ms. The PFG 3D ^{13}C-edited NOESY spectrum was recorded with 64 × 50 × 1024 complex data points in the t_1, t_2, and t_3 dimensions and 16 scans per increment. The spectral widths in the proton dimensions (t_1 and t_3) were 10 000 Hz, and the spectral width in the carbon dimension was 10 500 Hz.

Scalar $^3J(H^N-H^\alpha)$ coupling constants for [C40A, C95A] and wild-type RNase A were determined using the 3D PFG HNHA experiment (Kuboniwa et al., 1994). The spectra were acquired for wild-type and [C40A, C95A] RNase A using 50 × 42 × 1024 and 64 × 50 × 1024 complex data points in the t_1, t_2, and t_3 dimensions, respectively, and 16 or 24 scans per increment. The spectral widths in the proton dimensions (t_1 and t_3) were 6900 Hz, and the spectral width in the nitrogen dimension (t_2) was 2500 Hz. A dephasing period of 13.4 ms was used. The values of $^3J(H^N-H^\alpha)$ coupling constants were obtained from the intensity ratio of the cross-peaks to the diagonal peaks as described by Kuboniwa et al. (1994). Only those residues with resolved diagonal peaks were considered, and all values of $^3J(H^N-H^\alpha)$ were multiplied by a factor of 1.11 to account for relaxation effects as described by Vuister and Bax (1993).

All triple-resonance, 3D ^{15}N-edited, and 3D ^{13}C-edited spectra were processed with the FELIX (Molecular Simulations Inc.) software package on a Sun LX workstation using mirror-image linear prediction (Zhu & Bax, 1990) with 8 or 12 coefficients to double the duration of the t_1 and t_2 time domains. A Gaussian window function was applied in all three dimensions, and zero filling was used to extend the time−domain data further in the t_1 and t_2 dimensions to a final 3D matrix size of 256 × 256 × 1024 in the t_1, t_2, and t_3 dimensions. The ^{1}H, ^{13}C, and ^{15}N chemical shifts were referenced with 2,2-dimethyl-2-silapentane-5-sulfonic acid (DSS) as an internal standard using the protocol recommended by the IUPAC−IUBMB−IUPAB Interunion Task Group on NMR Data Bases (Wishart et al., 1995).

Backbone amide proton exchange rates for uniformly ^{15}N-enriched [C40A, C95A] RNase A were measured using PFG-HSQC spectra as described previously (Shimotakahara et al., 1997). Continuous sequential acquisition of 115 ^{15}N−^{1}H PFG-HSQC[1] spectra over a 3-day period was used to monitor amide ^{1}H/^{2}H exchange using lyophilized, protonated protein dissolved in ^2H_2O to a final concentration of 3.5 mM at pH* 4.60 ± 0.05 and 20 °C. All spectra were acquired with 192 × 2048 complex data points in the t_1 and t_2 dimensions and four scans per t_1 increment, using a total measurement time of 39 min per 2D spectrum. The 115 ^{15}N−^{1}H PFG-HSQC spectra were processed with identical baseline correction, Fourier transform, and peak picking parameters, using FELIX software coupled with semiautomated custom FELIX computer programs. The peak intensity as a function of time $I(t)$ and the rate constant (k) for each observed backbone amide ^{15}N−^{1}H resonance were calculated with Kaliedagraph (Synergy Software) using eq 1. The constant (C) was

$$I(t) = I_0 e^{-kt} + C \qquad (1)$$

included in the fit to account for the non-zero noise amplitude of the peak intensities measured in FELIX. The constant was bounded by the upper and lower limits of the observed intensity noise amplitude for each peak. The upper and lower limits were determined from the extrema of those data points (where each data point represents one ^{15}N−^{1}H PFG-HSQC spectrum) that had an average slope from an intensity vs time plot very close to zero.

Automated Analysis of Resonance Assignments. Automated peak picking and manual peak editing using FELIX software were carried out on a Sun LX workstation. Sequential backbone ^{1}H, ^{13}C, and ^{15}N and side-chain $^{13}C^\beta$ resonance assignments for ^{15}N,^{13}C-enriched [C40A, C95A] RNase A were determined on a Sun Sparc 10 workstation using the program AUTOASSIGN (Zimmerman et al., 1994, 1997). In a parallel study, we have reported the complete sequential assignment of backbone ^{1}H, ^{13}C, and ^{15}N and side-chain $^{13}C^\beta$ chemical shifts for uniformly ^{15}N,^{13}C-enriched wild-type and [C65S, C72S] RNase A (Shimotakahara et al., 1997). The automated analysis procedures used for these proteins were identical to those used for uniformly ^{15}N,^{13}C-enriched [C40A, C95A] RNase A in this study. Briefly, each backbone amide ^{1}H and ^{15}N resonance in both the 2D ^{15}N−^{1}H PFG-HSQC and the 3D PFG-HNCO spectra was established as a tentative root of generic (nonspecific amino acid type) spin systems (GSs). Cross-peaks in the other PFG triple-resonance experiments whose ^{1}H and ^{15}N resonance frequencies match the GS roots were then used to identify intraresidue [HN(CA)CO, HNCA, HA(CA)NH, and CBCANH], and interresidue [HNCO, CA(CO)NH, HA(CA)(CO)NH, and CBCA(CO)NH] connectivity information. Sequential connections between these spin systems were determined automatically, and the resulting linked segments of spin systems were mapped to unique segments of amino acids in the protein. In this way, AUTOASSIGN led to nearly complete sequence-specific backbone ^{1}H, ^{13}C, and ^{15}N and side-chain $^{13}C^\beta$ resonance assignments for ^{15}N,^{13}C-enriched [C40A, C95A] RNase A. The side-chain $^1H^\beta$, $^1H^\gamma$, $^1H^\delta$, $^1H^\epsilon$, and $^1H^\zeta$ resonance assignments for uniformly ^{15}N-enriched [C40A, C95A] RNase A were then determined

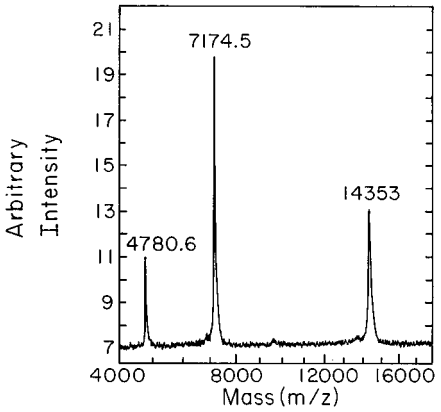

FIGURE 1: A MALDI-TOF MS spectrum for ^{15}N,^{13}C [C40A, C95A] RNase A.

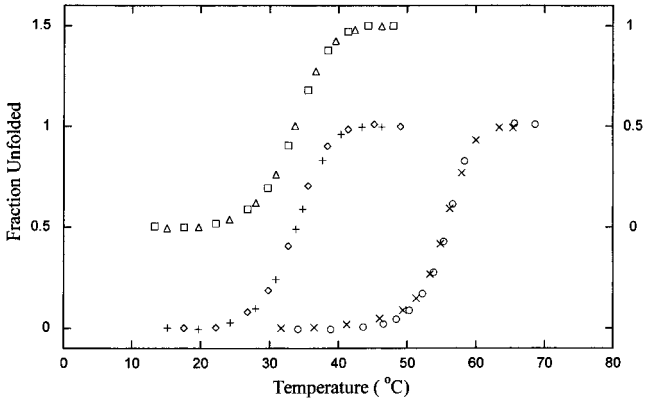

FIGURE 2: Thermal transition curves for [C40A, C95A], [C40S, C95S], and wild-type RNase A. [C40A, C95A] RNase A (◇, heating; +, cooling), [C40S, C95S] RNase A (□, heating; △, cooling), and wild-type RNase A (○, heating; ×, cooling) were dissolved in 100 mM sodium acetate, pH 4.60 ± 0.05. In order to display the data clearly, a constant of 0.5 was added to the value of the fraction unfolded for [C40S, C95S] RNase A. The left ordinate is the correct scale for [C40A, C95A] and wild-type RNase A, and the right ordinate is the correct scale for [C40S, C95S] RNase A. Data for wild-type RNase A are from Shimotakahara et al. (1997).

manually by extension of these backbone assignments using data from 3D ^{15}N-edited NOESY and 3D ^{15}N-edited TOCSY experiments.

RESULTS

Protein Characterization. All NMR samples were examined by N-terminal analysis, amino acid analysis, MALDI-TOF mass spectrometry, capillary electrophoresis (CE), and cation-exchange HPLC to determine sample homogeneity and purity. N-Terminal analysis confirmed that the first 20 residues of the samples were correct, and the amino acid analysis produced the expected amino acid composition of mutant and wild-type RNase A (N-terminal and amino acid analyses data not shown). Analyses of all NMR protein samples using CE and cation-exchange HPLC both *before* and *after* NMR experiments were also carried out to determine if significant chemical decomposition occurred during these measurements (CE and HPLC data not shown). Comparing the theoretical mass of ^{15}N,^{13}C-enriched [C40A, C95A] RNase A (14359 Da), assuming 99% ^{15}N and ^{13}C uniform enrichment, with the experimentally determined mass (14353 Da, Figure 1) reveals that the protein sample was ∼99% isotopically enriched in both ^{15}N and ^{13}C. Analysis of integrated peak areas from the chromatographs of ^{15}N,^{13}C-enriched [C40A,C95A] RNase A from both CE and HPLC reveal that the NMR protein sample was >99% homogeneous before NMR data collection and >97.5% homogeneous after 2 weeks of data collection (data not shown). Similar results were observed for uniformly ^{15}N-enriched wild-type and [C40A,C95A] RNase A samples used in 3D ^{15}N-edited, 3D HNHA, and $^{1}H/^{2}H$ NMR experiments (data not shown).

Comparison of Thermodynamic Properties and Enzymatic Activities of [C40A, C95A] and [C40S, C95S] RNase A. The reversible thermal transition curves of wild-type, [C40A, C95A], and [C40S, C95S] RNase A are shown in Figure 2. Thermodynamic properties, obtained from the curves in Figure 2, and enzymatic activities of the wild-type and two mutant proteins are given in Table 1. The value for the enthalpy of unfolding [$\Delta H°(T_m)$] for wild-type RNase A is consistent with values determined previously at pH 4.0 (Tsong et al., 1970; Privalov et al., 1973), and pH 4.6 (Talluri et al., 1994).

A small amount (1−5%) of irreversible denaturation was observed reproducibly in both mutant and wild-type RNase A thermal transitions. The extent of irreversible denaturation of wild-type RNase A has been determined previously to depend on the period of time that the protein solution is incubated at the higher temperatures during the heating and cooling process (Hermans & Scheraga, 1961). Therefore, denaturation and renaturation times were chosen which minimized the exposure of the protein solution to high temperature while allowing for thermal equilibration at each temperature (∼10 min). The errors in the thermodynamic parameters due to this irreversible denaturation are reflected in the respective uncertainties reported in Table 1.

The thermodynamic properties presented in Table 1 clearly indicate that disruption of the Cys40−Cys95 disulfide bond in RNase A destabilizes the protein. Moreover, replacement of both the Cys40 and Cys95 residues by either Ala or Ser appears to affect the stability of the mutant RNase A *equally* within experimental error. Moreover, the two disulfide mutants lacking the Cys40−Cys95 cross-link exhibited comparable enzymatic activities (Table 1), both of which were significantly lower than that of the native protein. Therefore, the destabilization of the three-disulfide mutants relative to the wild-type protein can be attributed to the inherent loss of the covalent disulfide cross-link rather than to the nature of the amino acid residues used to replace the native Cys40−Cys95 cross-link. The very similar thermodynamic properties and enzymatic activities of the [C40A, C95A] and [C40S, C95S] RNase A mutants demonstrate that both mutants are suitable analogs of the rate-determining folding intermediate, des-[40−95] RNase A. The [C40A, C95A] RNase A mutant was used for all subsequent NMR structural characterizations.

Backbone ^{1}H, ^{13}C, and ^{15}N and Side-Chain $^{13}C^{\beta}$ Resonance Assignments of [C40A, C95A] RNase A. Automated analysis of triple-resonance NMR data, obtained with uniformly ^{15}N,^{13}C-enriched [C40A, C95A] RNase A using the computer program AUTOASSIGN (Zimmerman et al., 1994, 1997), provided nearly complete sequential backbone ^{1}H, ^{13}C, and ^{15}N and side-chain $^{13}C^{\beta}$ resonance assignments of the protein. The execution time for AUTOASSIGN analysis of the peak-picked triple-resonance spectra was ∼6 min on a Sun Sparc

Table 1: Thermodynamic Properties for Unfolding and Relative Enzymatic Activities of Wild-Type, [C40A, C95A], and [C40S, C95S] RNase A at pH 4.60[a]

protein	T_m (°C)	$\Delta H°(T_m)$ (kcal/mol)	$\Delta S°(T_m)$ (eu)	enzymatic activity[f]
wild-type RNase A[b]	55.5 ± 0.2[c,d]	112 ± 5.0[e]	340 ± 16	100
[C40A, C95A] RNase A	33.7 ± 0.2	72.9 ± 3.7	238 ± 12	9 ± 4
[C40S, C95S] RNase A	33.6 ± 0.2	71.5 ± 1.8	231 ± 6.0	5 ± 3

[a] Thermal denaturation curves were determined at pH 4.60 ± 0.05. [b] Thermodynamic data for wild-type RNase A reported previously in a parallel study by Shimotakahara et al. (1997). [c] Uncertainties in T_m (°C) and $\Delta S°(T_m)$ are calculated from the errors in the *x*-intercept and slope of $\Delta G°(T)$ vs temperature (K) plots, respectively, in the transition region. [d] All uncertainties are reported at the 95% confidence limit. [e] Uncertainties in $\Delta H°(T_m)$ are calculated from the errors in van't Hoff plots. [f] Enzymatic activity at 22 °C relative to wild-type RNase A at pH 5.00 ± 0.05, measured using a cCMP substrate as described by Crook et al. (1960).

Table 2: Summary of AUTOASSIGN Analysis of Assignments for [C40A, C95A] RNase A

backbone and side-chain nuclei	no. of assignments possible[a]	automated analysis	subsequent manual analysis
$^1H^N$	119	115	119
^{15}N	119	115	119
$^{13}C'$	124	121	120
$^{13}C^\alpha$	124	120	123
$^1H^\alpha$	127	123	127
$^{13}C^\beta$	121	108	110

[a] Proline residues and the N-terminal lysine have no amide protons and thus no observable $^{15}N-^1H^N$ correlations. Glycine residues each have two H^α protons and no C^β resonances.

10 workstation. The assignments for [C40A, C95A] RNase A at pH 4.6 and 20 °C are tabulated in Table S1 (see Supporting Information), and a summary of some of the characteristics of the automated analysis is given in Table 2. Backbone amide proton and nitrogen chemical shifts are indicated on a plot of the 2D HSQC spectrum of [C40A, C95A] RNase A in Figure 3A. For clarity, the region of 113−122 ppm in the ^{15}N dimension (t_1) and 7.4−8.6 ppm in the ^1H dimension (t_2) is expanded in Figure 3B.

Backbone $^1H^N-^{15}N$ [C40A, C95A] RNase A resonance pairs which could not be resolved within the limits of the digital resolution of the 2D HSQC spectral data in Figure 3 were Asp53/Gln69 and Asn71/Tyr73. Assignments were derived for these "degenerate" residues by determining their respective generic spin systems (GSs) from the 3D HNCO data (Zimmerman et al., 1994, 1997). The amide proton and nitrogen chemical shifts in [C40A, C95A] RNase A generally had less dispersion than the corresponding chemical shifts in the wild-type protein (Shimotakahara et al., 1997), as indicated by the closely spaced resonances in the center of the 2D HSQC spectrum (Figure 3B). Poor chemical shift dispersion for [C40A, C95A] RNase A relative to the wild-type protein indicates a less ordered folded state for the mutant protein. Despite the fact that the N-terminal lysine and four proline residues in [C40A, C95A] RNase A have no amide protons, AUTOASSIGN was able to derive many of the $^{13}C'$, $^{13}C^\alpha$, $^1H^\alpha$, and side-chain $^{13}C^\beta$ resonance assignments for these residues from the triple-resonance data. Some manual peak editing was employed in an iterative manner to remove "spurious" peaks aligned with legitimate spin systems (Zimmerman et al., 1997).

In addition to the "spurious" peaks observed in the triple-resonance NMR data, a significant number of "minor peaks", typically ~10% of the intensity of the resonances assigned to the protein, were also observed in these data (see, for example, unassigned peaks in the center of the 2D HSQC spectrum; Figure 3B). These peaks, which were aligned with legitimate spin systems, were present even in freshly prepared

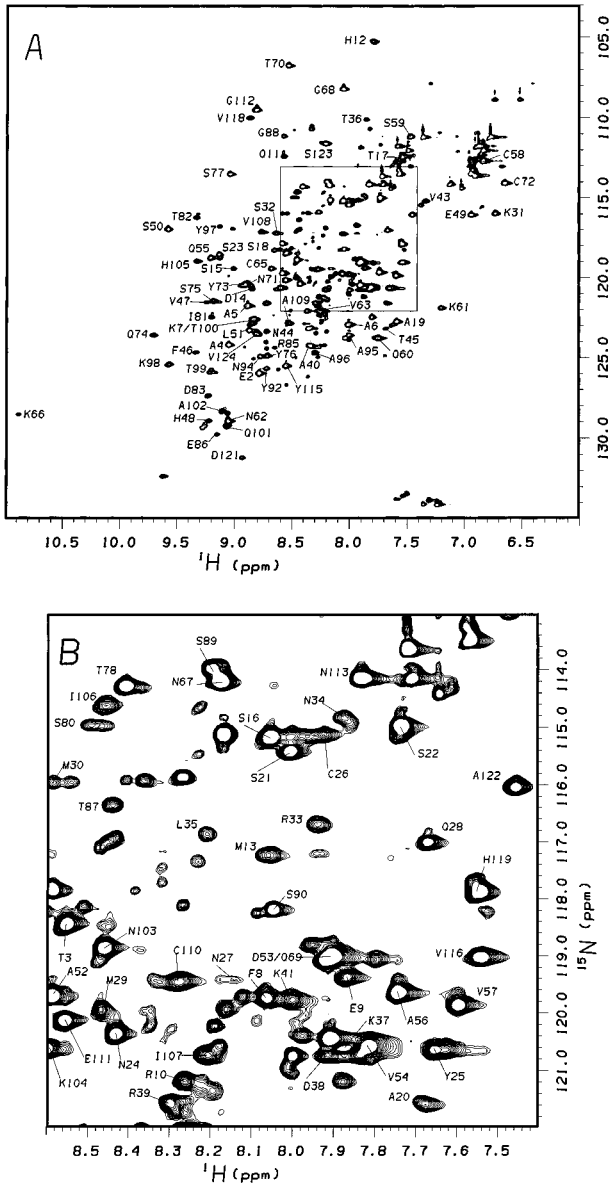

FIGURE 3: 2D PFG $^{15}N-$HSQC spectrum of uniformly ^{15}N-enriched [C40A, C95A] RNase A at pH* 4.60 ± 0.05 and 20 °C. The protein concentration was 4.5 mM, and 192 × 2048 complex points were acquired in the t_1 and t_2 dimensions with 96 scans per increment. To show the data more clearly, the boxed region in (A) is expanded in (B). Weak but observable $^{15}N-^1H^N$ correlations in the 2D PFG HSQC corresponding to C84 and F120 are not visible at the contour level presented in (A). Many weak resonances associated with minor conformational species are also present in these spectra.

protein samples and did not diminish or increase in intensity throughout data collection. Characterization of the chemical homogeneity of [C40A, C95A] RNase A both before and after triple-resonance experiments demonstrates that sample

impurities cannot account for these additional weak resonances. An alternative explanation for these extra peaks is the presence of "minor conformers" in [C40A, C95A] RNase A which exist in equilibrium with the major "native state" of the protein and which have a dynamic lifetime greater than ~1 ms. Similar observations of generally weaker resonances were reported for both [C65S, C72S] and wild-type RNase A (Shimotakahara et al., 1997), indicating that the presence of these extra resonances cannot be attributed to instability of the mutant protein. Such minor conformers might be attributed to non-native isomeric states of the four proline residues (Pro42, Pro93, Pro114, and Pro117). Ensembles of conformers of native proteins differing in X−Pro isomeric states have been observed in previous NMR studies (Evans et al., 1989; Chazin et al., 1989; Moy et al., 1995).

All [C40A, C95A] RNase A amide proton and nitrogen as well as α proton resonance assignments, with the exception of Phe120 and Tyr25, were confirmed independently from both 3D ^{15}N-edited NOESY and 3D ^{15}N-edited TOCSY experiments. In the 2D HSQC spectrum, Phe120 has a weak ^{1}H−^{15}N correlation and is too weak to be observed in the 3D ^{15}N-edited NOESY and 3D ^{15}N-edited TOCSY spectra. Moreover, Tyr25 was observed only in the 3D ^{15}N-edited NOESY spectrum.

Chemical Shift Comparison between Wild-Type and [C40A, C95A] RNase A. Individual protein residue chemical shifts depend strongly on local chemical and electronic environments. Therefore, direct comparisons of chemical shift data between [C40A, C95A] and wild-type RNase A can elucidate local areas within the mutant protein where structural alterations are present. Accordingly, a comparison of assigned backbone ^{1}H^{N}, ^{15}N, ^{13}C′, ^{13}C$^{\alpha}$, and side-chain ^{13}C$^{\beta}$ chemical shifts for uniformly ^{15}N,^{13}C-enriched wild-type (Shimotakahara et al., 1997) and [C40A,C95A] RNase A is shown in Figure 4. As might be expected, the largest chemical shift differences between mutant and wild-type RNase A are centered around the two polypeptide segments encompassing Asn34−Thr45 and Asp83−Gln101 of the mutant protein where the native Cys40−Cys95 cross-link was removed. Within these two polypeptide segments in the wild-type protein are three β-strands[2] (strands β1, β4, and β5) which collectively form the antiparallel β-sheet 1 (Santoro et al., 1993; Wlodawer et al., 1988). Such pronounced chemical shift differences (Figure 4) in these polypeptide segments indicate significant structural perturbations in the regions of this triple-stranded β-sheet structure spatially adjacent to the mutation sites in [C40A, C95A] RNase A. In wild-type RNase A, the Cys40−Cys95 disulfide bond joins together two looped structures of the protein (one of which is a type VI β-turn between β4 and β5) spatially distant from each other in the primary sequence. It appears from the chemical shift data in Figure 4 that the removal of the Cys40−Cys95 cross-link of RNase A also results in structural and/or dynamic perturbations of these polypeptide loop structures.

Backbone ^{1}H^{N}, ^{15}N, ^{13}C′, ^{13}C$^{\alpha}$, and side-chain ^{13}C$^{\beta}$ chemical shift deviations between wild-type and [C40A, C95A] RNase A are also observed throughout much of the protein, even in regions *distant in space* from the disulfide mutation sites. Individual residue chemical shift difference data for ^{1}H^{N}, ^{15}N, and ^{13}C$^{\alpha}$ are represented on ribbon drawings of wild-type RNase A in Figure 5. Significant ^{1}H^{N} ($\Delta\delta \geq 0.1$ ppm) and ^{15}N ($\Delta\delta \geq 1.0$ ppm) chemical shift differences between wild-type and [C40A, C95A] RNase A were observed for most residues in β-sheet 1 and some residues in β-sheet 2 of the mutant RNase A (Figure 5A,B). The digital resolutions of the corresponding triple-resonance NMR experiments were 0.014, 0.19, 0.023, 0.063, and 0.31 ppm for ^{1}H^{N}, ^{15}N, ^{13}C$^{\alpha}$, ^{13}C′, and ^{13}C$^{\beta}$ nuclei, respectively. Significantly, numerous other residues in β-sheet 2 of the mutant protein exhibited subtle ^{1}H^{N} ($\Delta\delta \geq 3\times$ the digital resolution) and ^{15}N ($\Delta\delta \geq 2\times$ the digital resolution) chemical shift differences (Figure 5A,B). Similarly, subtle ^{1}H^{N} and ^{15}N chemical shift differences between wild-type and mutant RNase A were also evident in the polypeptide region Lys1−Arg33 of [C40A, C95A] RNase A (Figure 5A,B), which is not adjacent to the Cys40 → Ala40 mutation site. In the wild-type protein, this region encompasses two α-helices (α1 and α2) and an intervening polypeptide sequence with no regular secondary structure. It is worth noting that the polypeptide segments of [C40A, C95A] RNase A most similar to the wild-type protein in terms of backbone ^{1}H,

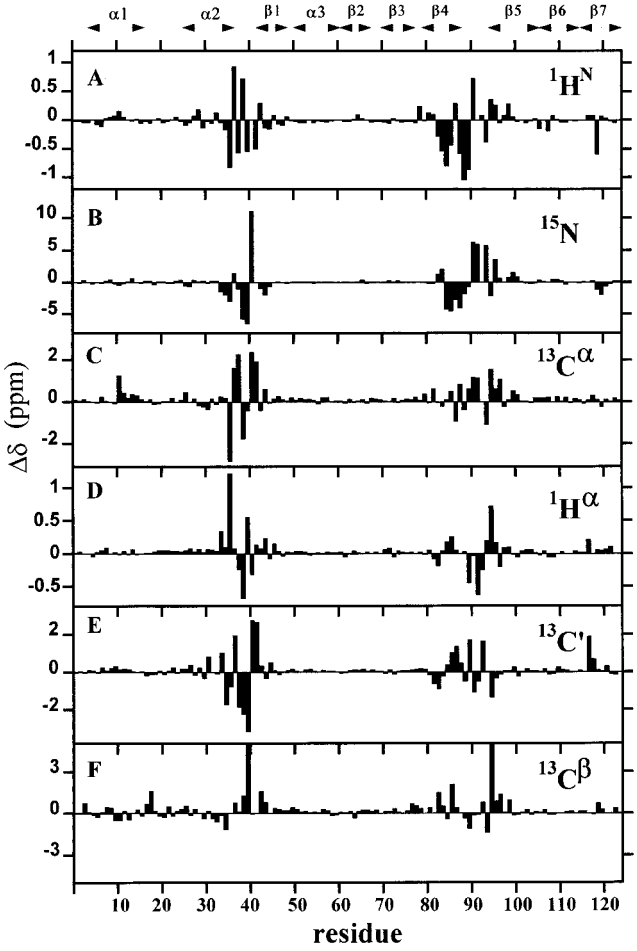

FIGURE 4: Chemical shift differences ($\Delta\delta = \delta_{\text{wild-type}} - \delta_{\text{[C40A,C95A]}}$) between wild-type (Shimotakahara et al., 1997) and [C40A, C95A] RNase A for ^{1}H^{N} (A), ^{15}N (B), ^{13}C$^{\alpha}$ (C), ^{1}H$^{\alpha}$ (D), ^{13}C′ (E), and ^{13}C$^{\beta}$ (F), respectively, as a function of residue number. Backbone α-helix and β-sheet structures indicated by arrows above the plots are based on the X-ray crystal structure of RNase A (Wlodawer et al., 1988).

[2] The designations of β-sheet used in this study are based on the locations of β-strands reported in the Brookhaven Protein Data Bank (PDB) entry 9RSA: β1, sheet 1, strand 1; β2, sheet 2, strand 1; β3, sheet 2, strand 2; β4, sheet 1, strand 2; β5, sheet 1, strand 3; β6, sheet 2, strand 3; and β7, sheet 2, strand 4.

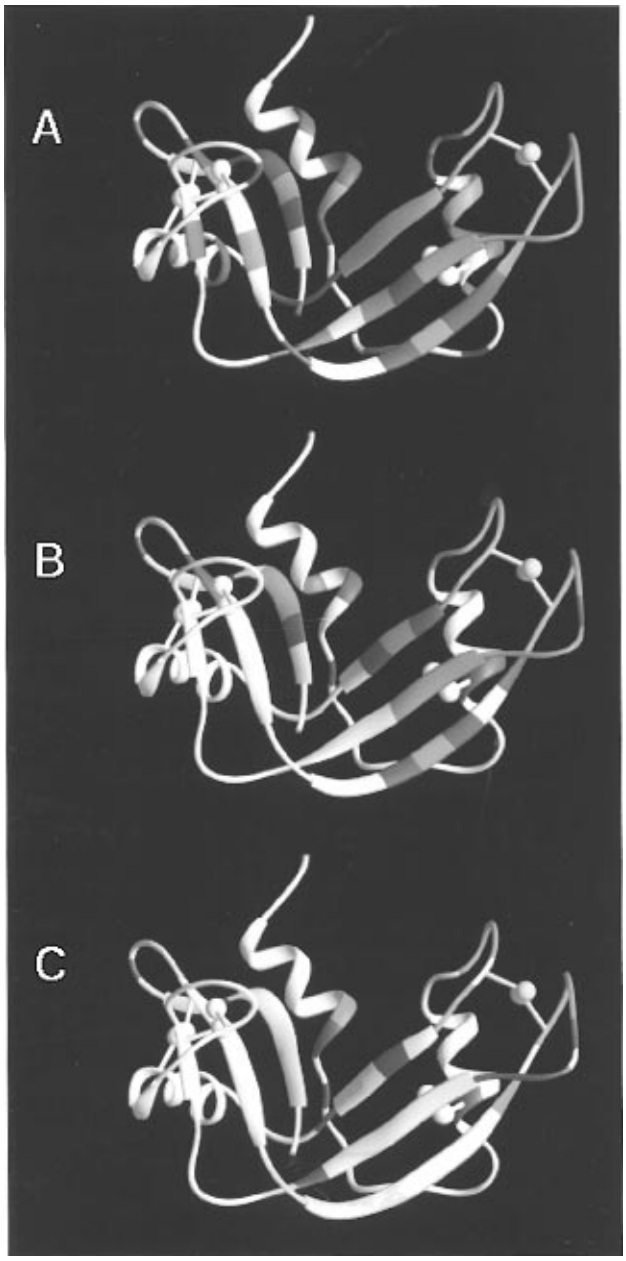

FIGURE 5: Ribbon representation of wild-type RNase A with regions of the protein exhibiting significant chemical shift deviations of [C40A, C95A] RNase A from the wild-type protein indicated in red (A, $^1H^N$ $\Delta\delta \geq 0.1$; B, ^{15}N $\Delta\delta \geq 1.0$; C, $^{13}C^\alpha \geq 1.0$) and those regions with subtle differences indicated in blue (A, $^1H^N$ $\Delta\delta \geq 3\times$ digital resolution; B, ^{15}N $\Delta\delta \geq 2\times$ digital resolution; C, $^{13}C^\alpha$ 2 $\times$ digital resolution). Residues with no corresponding resonance assignment are indicated in gray. The four native disulfide bonds in wild-type RNase A are indicated in white (C26−C84, C58−C110, and C65−C72) and yellow (C40−C95), respectively. The RNase A structure shown is based on the atomic coordinates obtained from the Brookhaven Protein Data Bank entry 9RSA (Wlodawer et al., 1988).

^{15}N, and ^{13}C chemical shift deviations are also the most spatially distant region of the protein from the two mutation sites (Figure 5).

Determination of $^3J(H^N-H^\alpha)$ Coupling Constants for Wild-Type and [C40A, C95A] RNase A. $^3J(H^N-H^\alpha)$ coupling constants for wild-type and [C40A, C95A] RNase A, determined from 3D HNHA data, are presented in Table S2 (Supporting Information). In all, 86 and 56 $^3J(H^N-H^\alpha)$ coupling constants were determined for wild-type and mutant RNase A, respectively. Comparing the values for wild-type RNase A from 3D HNHA with those of Shimotakahara et al. (1997) determined by using PFG-HMQC-J (Kuboniwa et al., 1994), the average difference $[^3J(H^N-H^\alpha)_{3D\ HNHA} - {}^3J(H^N-H^\alpha)_{2D\ HMQC-J}]$ was −0.70 Hz, which was similar to that reported previously (−0.63 Hz) for calcium-free calmodulin by Kuboniwa et al. (1994). After correction for this systematic difference in measured $^3J(H^N-H^\alpha)$, the precision of the values for the wild-type RNase A coupling constants were estimated as ±0.5 Hz for values of $^3J(H^N-H^\alpha)$ greater than ∼5 Hz. However, back calculation of $^3J(H^N-H^\alpha)$ coupling constants from 1.26 Å X-ray data (Wlodawer et al., 1988) using the Karplus curve described by Pardi et al. (1984) reveals that the differences between measured values from RNase A in solution and back-calculated values can be ±1.5 Hz for $^3J(H^N-H^\alpha)$ values greater than ∼5 Hz and somewhat larger for smaller values of $^3J(H^N-H^\alpha)$ (Shimotakahara et al., 1997). Accordingly, only those differences in $^3J(H^N-H^\alpha)$ coupling constants between mutant and wild-type RNase A greater than 1.5 Hz were considered significant. Using this criterion, 12 out of the 56 values of $^3J(H^N-H^\alpha)$ determined for both forms of RNase A were significantly different (Ala6, Arg10, Leu35, Thr36, Arg39, Cys40/Ala40, Ser59, Val63, Asp83, Lys91, Ile107, and Val108; Table S2, Supporting Information).

Isomeric State of the X−Pro93 Peptide Bond in [C40A, C95A] RNase A. Since the Tyr92−Pro93 dipeptide sequence is believed to be part of a chain folding initiation site (CFIS) in wild-type RNase A, it is of interest to determine the isomeric state of the corresponding peptide bond in both the mutant and wild-type proteins. Generally, backbone $^{13}C^\beta$ chemical shifts of cis and trans isomers of proline residues are significantly different ($\Delta^{13}C^\beta_{cis-trans}$ ∼2.6 ppm in a statistical coil; Thanabal et al., 1994) and can be used to identify the isomeric states of X−Pro peptide bonds. For both mutant and wild-type RNase A, the $^{13}C^\beta$ chemical shifts of Pro93 are within 0.5 ppm of that which is observed for a cis-proline conformation in a statistical coil. Moreover, the difference between the wild-type and [C40A, C95A] RNase A backbone $^{13}C^\beta$ chemical shifts for Pro93 is only 0.7 ppm. These chemical shift data indicate that the Tyr92−Pro93 peptide bond is in the cis conformation in both wild-type *and* mutant RNase A. Further evidence for a cis Tyr92−Pro93 peptide bond in [C40A, C95A] RNase A comes from an $^1H^\alpha_i-{}^1H^\alpha_{i-1}$ NOE, observed in the 3D ^{13}C-edited spectrum of [C40A, C95A] RNase A, between these two residues. The internuclear distance between α protons in a cis X−Pro peptide is less than 4 Å (Talluri et al., 1987), and therefore, an NOE is theoretically observable. Conversely, in a trans X−Pro peptide the $^1H^\alpha_i-{}^1H^\alpha_{i-1}$ distance is greater than 5 Å (Talluri et al., 1987), which cannot be detected using the NOE data presented here. Therefore, $^1H^\alpha-{}^1H^\alpha$ NOE's are not expected for Lys41−Pro42 and Val116−Pro117 (trans peptide bonds) in the mutant RNase A unless these adopt cis peptide conformations at either position in the amino acid sequence. Unfortunately, $^{13}C^\beta$ resonance assignments were not determined for the other three proline residues (Pro42, Pro114, and Pro117) in the mutant RNase A, and no resolved X−Pro $^1H^\alpha_i-{}^1H^\alpha_{i-1}$ NOE's were identified; hence the isomeric states of these other X−Pro peptide bonds in [C40A, C95A] RNase A could not be determined.

Relative Backbone Amide Proton Exchange Rates in Mutant and Wild-Type RNase A. Backbone amide protons in both mutant and wild-type RNase A which are "protected"

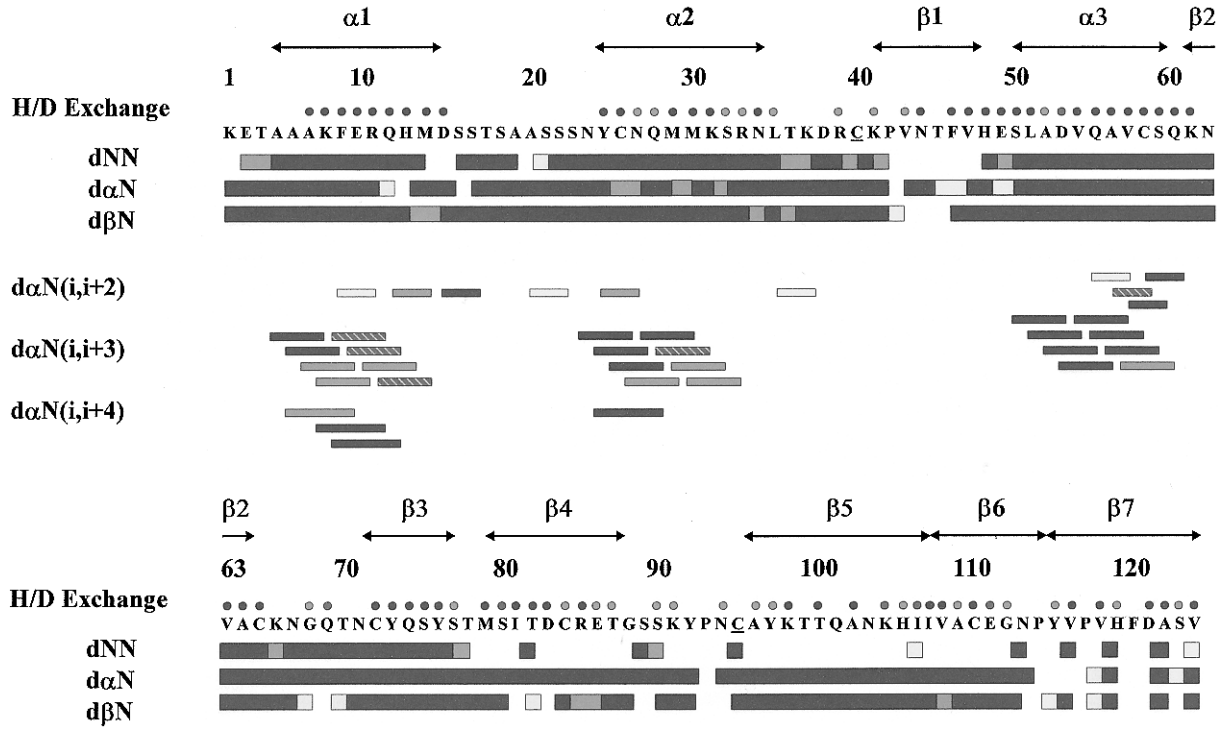

FIGURE 6: Survey of protected amide protons (circles) and both short-range and medium-range NOE's involving $^1H^N$ protons (rectangles) for [C40A, C95A] and wild-type RNase A at pH* 4.60 and 20 °C. Protected amide protons were identified by a corresponding $^1H-^{15}N$ correlation observed in the first 2D HSQC spectrum ($k < \sim 0.02\ s^{-1}$). Blue circles indicate that the corresponding amide proton resonance was observed in the $^1H/^2H$ exchange experiments in both mutant and wild-type RNase A samples, red circles indicate that the corresponding amide proton resonance was observed only in wild-type RNase A, while green circles indicate that the corresponding amide proton was observed in wild-type RNase A and in the mutant, but that the $^1H^N$ assignment in the 2D HSQC spectrum of the mutant (Asp53 and/or Gln69, Ser80 and/or Ile106) or wild-type (K104 and/or Glu111) protein was ambiguous. Similarly, blue rectangles indicate that the corresponding NOE's were observed in both mutant and wild-type RNase A, while those in red and yellow were observed only in wild-type and [C40A, C95A] RNase A, respectively. Hatched green rectangles indicate that the corresponding NOE was observed in both wild-type and [C40A, C95A] RNase A, but that either the mutant or wild-type resonance assignment was ambiguous because of spectral overlap. Secondary structure, based on the X-ray crystal structure of RNase A (Wlodawer et al. 1988), is indicated schematically by arrows above the amino acid sequence. Locations in the amino acid sequence where mutated cysteines were replaced by alanines in [C40A, C95A] RNase A are underlined.

are defined as those for which $^1H-^{15}N$ correlations were observed in 2D PFG HSQC spectra recorded within 50 min of dissolving the protein in ^2H_2O at pH* 4.60 and 20 °C (10 min for sample preparation and 40 min for data collection). The fastest $^1H_2O/^2H_2O$ amide proton exchange rate constant (k) observable using these NMR data was $\sim 0.02\ s^{-1}$. Figure 6 reveals that 83 unambiguously determined protected amide protons were identified in wild-type RNase A, indicated by blue, red, and green circles (plus Lys104 and/or Glu11 indicated by green circles in Figure 6) (Shimotakahara et al., 1997). In contrast, using this criterion, only 56 protected amide protons, indicated by blue and green circles in Figure 6 (plus Asp53 and/or Gln69 and Ser80 and/or Ile106 indicated by green circles in Figure 6), were identified in [C40A, C95A] RNase A. A comparison of relative backbone amide $^1H/^2H$ exchange rate constants measured for wild-type and [C40A, C95A] RNase A at 20 °C and pH* 4.6 is presented in Figure 7. Residues in the respective proteins exhibiting large [$\log(k_{wild-type}/k_{[C40A,\ C95A]}) > 4$], moderate [$4 \geq \log(k_{wild-type}/k_{[C40A,C95A]}) > 1$], and small [$\log(k_{wild-type}/k_{[C40A,C95A]}) \leq 1$] differences in relative amide exchange rate constants are also indicated on a ribbon structure of the wild-type protein in Figure 8. It is evident from these data that the global stability of the mutant RNase A is significantly affected by the loss of the native Cys40−Cys95 cross-link. Moreover, Figures 7 and 8 reveal that the largest differences in relative backbone amide exchange rate constants between the mutant and wild-type protein ($k_{wild-type}/k_{[C40A,C95A]} = 10^4-10^6$), with the exception of Met30, are located in either the third α-helix (α3) or the two β-sheet structures present in wild-type RNase A. It is worth noting, however, that most backbone amide protons located in the two N-terminal α-helices (α1 and α2) of wild-type RNase A that exhibit only moderate protection ($k_{wild-type} = 10^3-10^7\ s^{-1}$) also exhibit 10−300-fold relative increases in $^1H/^2H$ exchange rate constants in the mutant protein (Figures 7 and 8).

Side-Chain Assignments of [C40A, C95A] RNase A. Side-chain $^1H^\beta$, $^1H^\gamma$, $^1H^\delta$, $^1H^\epsilon$, and $^1H^\zeta$ for uniformly ^{15}N-enriched [C40A, C95A] RNase A, determined at pH 4.6 and 20 °C using data from both 3D ^{15}N-edited NOESY and 3D ^{15}N-edited TOCSY experiments, are tabulated in Table S3 (Supporting Information). Resonance assignments of side-chain residues not close to either mutation site were generally in good agreement with published wild-type assignments (Robertson et al., 1989; Rico et al., 1989; Santoro et al., 1993), further indicating that the overall global chain fold of [C40A, C95A] RNase A is similar to that of wild-type RNase A.

Comparison of Backbone Secondary Structures between [C40A, C95A] and Wild-Type RNase A. A summary of all backbone $^{13}C^\alpha$ chemical shift deviations from statistical-coil values ($\Delta^{13}C^\alpha$) (Thanabal et al., 1994) is presented, for both the wild-type and mutant protein, in Figure 9. Values of $\Delta^{13}C^\alpha$ provide a qualitative characterization of ϕ, ψ backbone

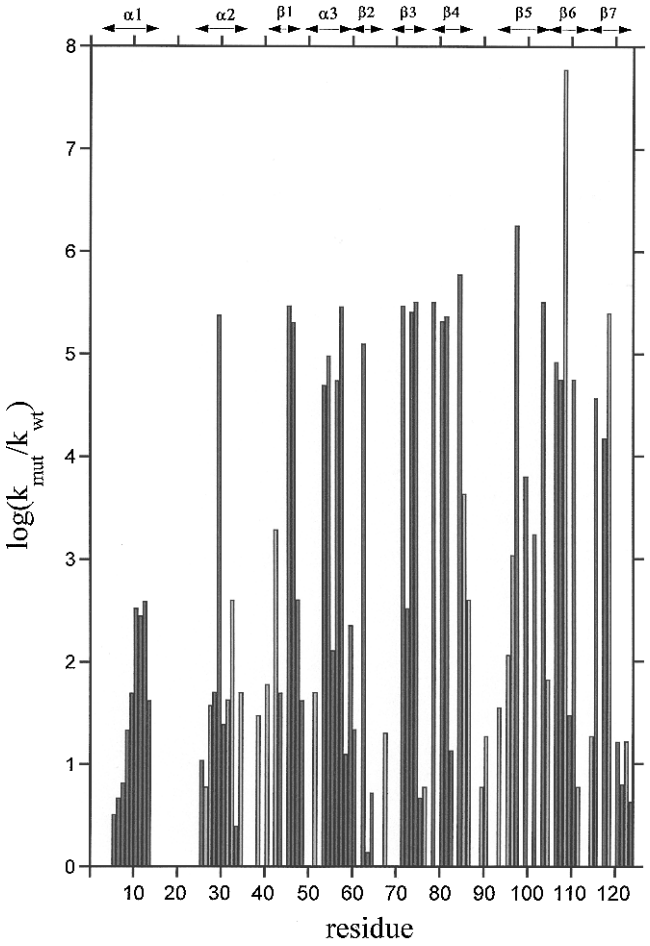

FIGURE 7: Relative $^1H/^2H$ amide proton exchange rate constants $\log(k_{wild-type}/k_{[C40A,C95A]})$ for wild-type and [C40A, C95A] RNase A at pH 4.60 ± 0.05 and 20 °C. Residues in which exchange rate constants were unambiguously determined for both mutant and wild-type RNase A are indicated by blue bars. In order to determine the *minimum* relative change in amide proton exchange rate constants for those residues which had observable amide resonances in the wild-type but *not in the mutant protein*, a value of 0.02 s^{-1} (the largest observable exchange rate for the experimental method used in this study) was used for these residues in the mutant; such residues are indicated by red bars. Wild-type RNase A amide $^1H/^2H$ exchange rate constants used in the comparison were those reported by Shimotakahara et al. (1997). Arrows above the plot indicate elements of secondary structure observed in the wild-type protein (Wlodawer et al., 1988).

FIGURE 8: Color classification of the magnitude of the observed relative $^1H/^2H$ exchange rate constants for wild-type and [C40A, C95A] RNase A superimposed on a ribbon representation of the wild-type protein. Residues with relative $^1H/^2H$ exchange rate constants of $\log(k_{wild-type}/k_{[C40A,C95A]}) > 4$ are indicated in blue, those of $4 \geq \log(k_{wild-type}/k_{[C40A,C95A]}) > 1$ are indicated in red, and those of $\log(k_{wild-type}/k_{[C40A,C95A]}) \leq 1$ are indicated in green.

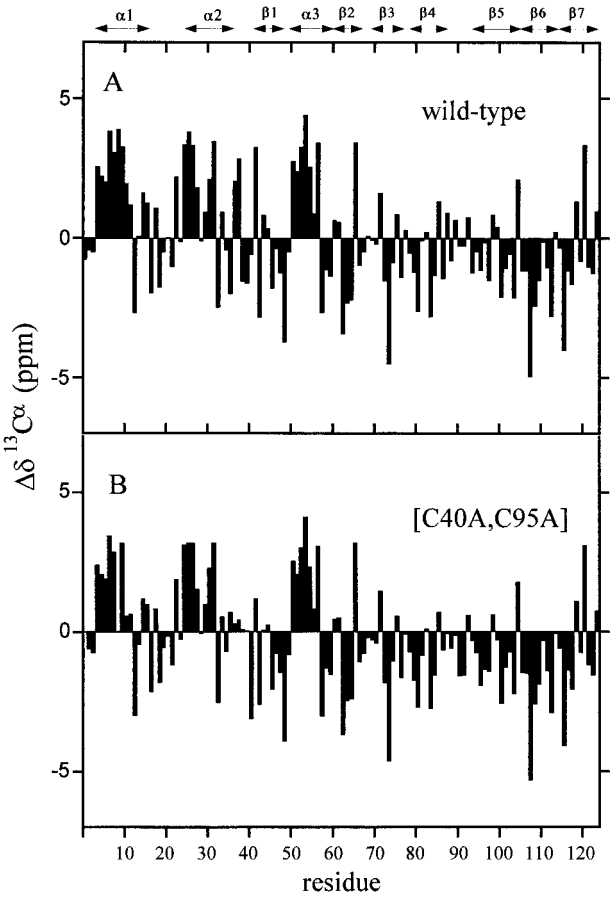

FIGURE 9: Comparison of $^{13}C^\alpha$ chemical shift deviations from statistical coil values ($\Delta\delta = \delta C^\alpha_{obs} - \delta C^\alpha_{coil}$). Differences are plotted as a function of residue number for wild-type (A) and [C40A, C95A] RNase A (B). Backbone α-helix and β-sheet structures indicated by arrows above the plots are based on the X-ray crystal structure of RNase A (Wlodawer et al., 1988).

conformations in proteins (Spera & Bax, 1991). The overall similarity between the $^{13}C^\alpha$ chemical shift differences for [C40A, C95A] and wild-type RNase A is striking. At first sight, these $\Delta\delta C^\alpha$ chemical shift data might seem to contradict the backbone $^1H^N$, ^{15}N, $^{13}C'$, $^{13}C^\alpha$, and side-chain $^{13}C^\beta$ chemical shift difference ($\Delta\delta = \delta_{wild-type} - \delta_{[C40A,C95A]}$) data presented in Figures 4 and 5, since most of the major secondary structural elements (α-helices and β-sheets characterized by positive and negative values of $\Delta^{13}C^\alpha$, respectively) appear to be present in both [C40A, C95A] and wild-type RNase A (Figure 6). However, subtle $\Delta\delta C^\alpha$ chemical shift differences between [C40A, C95A] and wild-type RNase A can be seen in Figure 9 in the regions of the three strands of β-sheet 1 (β1, β4, and β5) and of both the loop polypeptide sequences which are spatially adjacent to the Cys40−Cys95 mutation site. Accordingly, the *similar* $\Delta\delta C^\alpha$ chemical shift differences (Figure 9) coupled with the *statistically significant* backbone and side-chain chemical shift differences between [C40A, C95A] and wild-type RNase A present throughout the protein in regions not adjacent to the Cys40−Cys95 mutation site (especially polypeptide regions Lys1−Arg33 and Gln101−Val124; Figure 5) indicate subtle, delocalized structural or dynamic

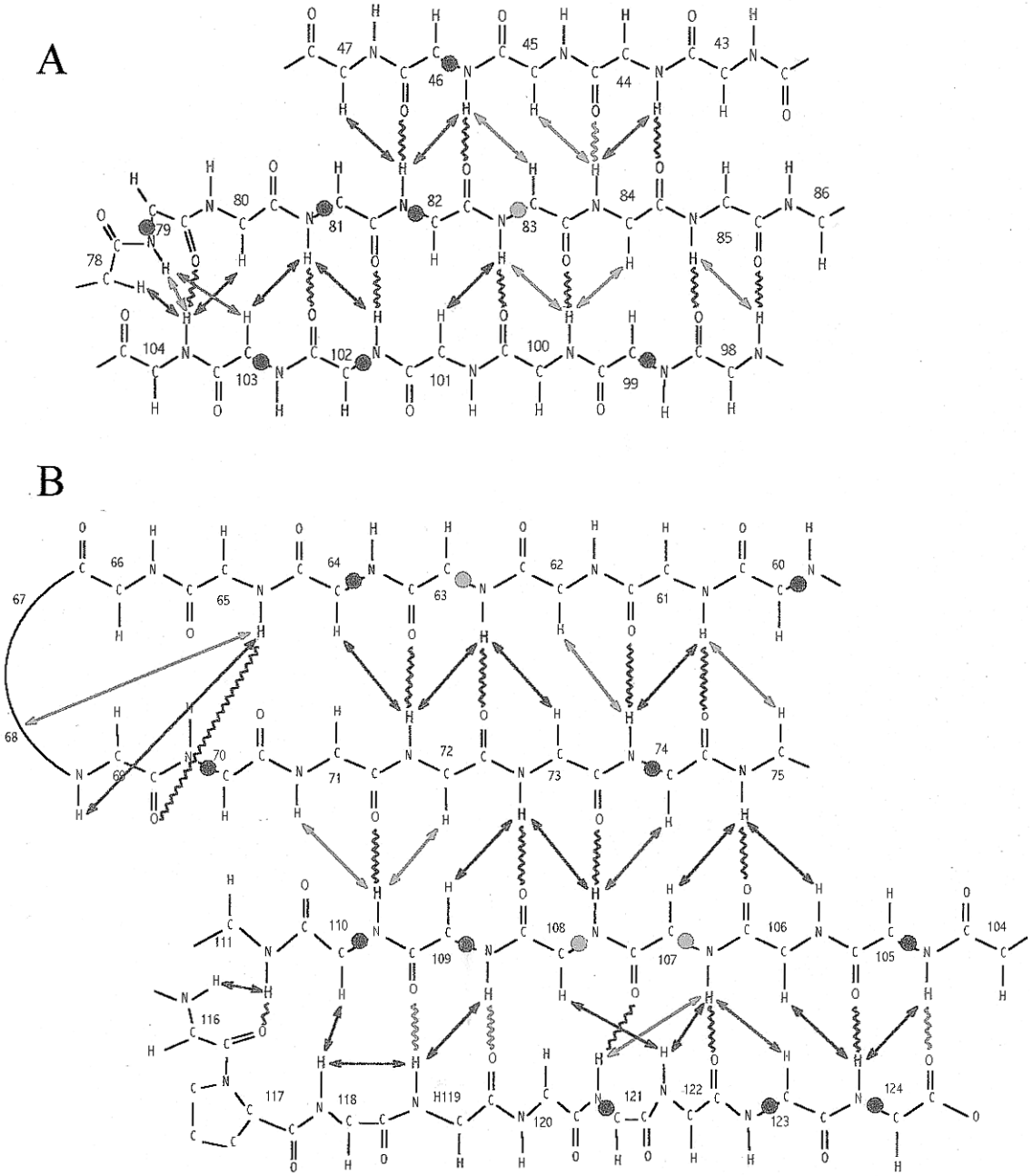

FIGURE 10: Protected amide protons and short internuclear distances in wild-type and [C40A, C95A] RNase A superimposed on a schematic representation of the X-ray structure of the two major β-sheets (β-sheet 1, A; β-sheet 2, B) of wild-type RNase A (Wlodawer et al., 1988). Blue wavy lines and double-headed arrows indicate that the corresponding protected amide protons and short internuclear distances were observed in both wild-type and [C40A, C95A] RNase A as determined by $^1H/^2H$ exchange and 3D ^{15}N-edited NOESY experiments, respectively. Wavy lines and double-headed arrows in red indicate that the corresponding protected amide protons and short internuclear distances were observed only in wild-type RNase A, while wavy lines and double-headed arrows in green indicate that the corresponding protected amide protons and short internuclear distances were observed in both wild-type and [C40A, C95A] RNase A, but one of the $^1H^N-^{15}N$ or $^1H^\alpha$ resonance assignments in the mutant or wild-type protein was ambiguous because of overlap with other peaks in the NMR spectrum. Blue circles indicate that the measured $^3J(^1H^N-H^\alpha)$ coupling constants for the corresponding residue in wild-type and mutant RNase A were similar ($|\Delta J| \leq 1.5$ Hz), while those indicated in red were significantly different ($|\Delta J| > 1.5$ Hz) between the two proteins.

perturbations throughout the structure of [C40A, C95A] RNase A.

A survey of all short-range and medium-range NOE's between H^N, H^α, and H^β protons, together with a summary of the locations of slowly exchanging backbone amide protons observed in mutant and wild-type RNase A, is presented in Figure 6. A schematic representation of the two major β-sheet structures (β-sheet 1, A; β-sheet 2, B) of RNase A (Wlodawer et al., 1988) showing locations of protected amide protons and comparisons of $^3J(H^N-H^\alpha)$ coupling constants and interstrand NOE's observed in wild-type and [C40A, C95A] RNase A are shown in Figure 10. The $^1H/^2H$ and NOE data shown in Figures 6 and 10 demonstrate the overall similarity in backbone structures of [C40A, C95A] and wild-type RNase A. Many $^1H^N_i-^1H^\alpha_{i-3}$ NOE's, characteristic of α-helical structure in proteins, and protected amide protons, consistent with helical hydrogen bonds, are observed in both mutant and wild-type proteins in the regions where the three α-helices (α1, Thr3−Met13; α2, Asn24−Asn34; and α3, Ser50−Gln60) are present in wild-type RNase A (Figure 6; Wlodawer et al., 1988; Santoro et al., 1993). Moreover, the $\Delta\delta C^\alpha$ values for [C40A, C95A]

RNase A indicate α-helices ($\Delta\delta C^{\alpha} > 0$) and β-sheets ($\Delta\delta C^{\alpha} < 0$) in regions where such secondary structures are located in the wild-type protein.

The $^1H/^2H$ exchange and NOE data presented in Figures 6 and 10 do, however, indicate numerous *potentially* disrupted hydrogen bonds scattered throughout the major secondary structures of [C40A, C95A] RNase A, as well as more profound structural perturbations in the regions of the protein adjacent to the disulfide mutation sites. Specifically, Figure 6 reveals that 10 backbone amides that are protected in wild-type RNase A (red circles) adjacent to the two mutation sites [Cys40 (Leu35, Arg39, Lys41, and Val43) and Cys95 (Glu86, Thr87, Ser90, Lys91, Asn94, Ala96, and Tyr97)] were not sufficiently slowly exchanging to be observed in [C40A, C95A] RNase A. Furthermore, the first two N-terminal α-helices (α1 and α2) in the primary sequence of [C40A, C95A] RNase A appear to be affected by the loss of the Cys40−Cys95 disulfide cross-link, as evidenced by the absence of nearly half of the $^1H^N_i-^1H^{\alpha}_{i-3}$ NOE's observed in the wild-type protein (Figure 6). Moreover, significant deviations in $^3J(H^N-H^{\alpha})$ coupling constants are observed for residues Ala6 ($|\Delta J| = -1.6$ Hz) and Arg10 ($|\Delta J| = -3.9$ Hz) in the N-terminal α-helix (α1) of [C40A, C95A] RNase A compared to the corresponding values in the wild-type protein. In addition, four amide protons characterized as "protected" in the second α-helix (α2, Asn27, Gln28, Ser32, and Arg33) observed in wild-type RNase A are not observed as slowly exchanging in the mutant protein.

Four amide protons which do not exhibit detectable solvent protection in [C40A, C95A] RNase A contribute to the interstrand β-sheet hydrogen-bonding network in wild-type RNase A (Figure 10A; β-sheet 1, Cys84; Figure 10B; β-sheet 2, His105, Ala109, and His119). Figure 10 also reveals that six interstrand NOE's in each β-sheet, which are observed in wild-type RNase A, are not observed in the mutant protein. More generally, consistent with the global destabilization or delocalized structural perturbation of [C40A, C95A] RNase A, the more rapidly exchanging amide protons and NOE cross-peaks in the mutant protein are distributed throughout most of the amino acid sequence (Figures 6 and 10), with the polypeptide segment in the middle of the sequence (Ser50−Ser75) being affected the least and the two polypeptide regions encompassing the mutation sites (Arg33−Thr45 and Asp83−Thr100) being affected the most.

DISCUSSION

An analog of the rate-determining intermediate in the major oxidative folding and reduction pathways of RNase A, [C40A, C95A] RNase A, has been characterized extensively in terms of backbone structure and thermodynamic stability. Similar data involving a blocked analog (Talluri et al., 1994) and, more recently, a mutant analog, [C65S, C72S] of RNase A (Shimotakahara et al., 1997), have been reported. Since two independent pathways are observed in the regeneration (Rothwarf & Scheraga, 1991, 1993a−d; Rothwarf et al., 1995) and reduction (Li et al., 1995) of RNase A in the presence of DTT, the major pathway through des-[40−95] and the minor pathway through des-[65−72], these data provide important complementary information regarding details of folding and unfolding pathways of the wild-type protein.

Automated Analysis of Resonance Assignments. An assignment of nearly all backbone $^1H^N$, ^{15}N, $^1H^{\alpha}$, $^{13}C^{\alpha}$, and $^{13}C'$ and most $^{13}C^{\beta}$ resonance assignments was achieved in approximately 2 weeks, considering the time required to collect, process, and peak-pick the NMR data. Analysis time using AUTOASSIGN was minimal (∼6 min). Moreover, no information from wild-type resonance assignments was used in the automated analysis. These resonance assignments were generally in good agreement with the corresponding $^1H^N$ and $^1H^{\alpha}$ assignments of the wild-type protein reported by Robertson et al. (1989), Rico et al. (1989), and Santoro et al. (1993) and, more recently, with the $^1H^N$, ^{15}N, $^1H^{\alpha}$, $^{13}C^{\alpha}$, $^{13}C'$, and $^{13}C^{\beta}$ assignments reported by Shimotakahara et al. (1997) in the regions spatially distant from the Ala40 and Ala95 mutation sites.

Comparison of Wild-Type and Mutant Chain Folds from Chemical Shift Data. Direct comparisons of chemical shift data between [C40A, C95A] and wild-type RNase A indicated that the two localized regions spatially adjacent to the Ala40 and Ala95 mutation sites in the mutant protein exhibit significant localized perturbations (Figure 4). However, the remarkable similarity of the $^{13}C^{\alpha}$ chemical shift deviations from statistical coil values ($\Delta^{13}C^{\alpha}$) between the mutant and wild-type proteins in regions distant in the amino acid sequence from the Ala40 and Ala95 mutation sites indicates that the overall chain folds of [C40A, C95A] and wild-type RNase A are also quite similar (Figure 9). Furthermore, comparison of Figure 5A with Figure 5C reveals greater chemical shift differences between mutant and wild-type RNase A in $^1H^N$ resonances than the corresponding $^{13}C^{\alpha}$ resonances in regions distant from the Cys40 → Ala and Cys95 → Ala mutation sites. Amide $^1H^N$ chemical shifts are more sensitive to backbone hydrogen-bonding perturbations due to changes in thermodynamic and/or dynamic fluctuations, whereas $^{13}C^{\alpha}$ chemical shifts are more dependent on backbone conformation (in terms of ϕ, ψ values). Consequently, comparisons between mutant and wild-type RNase A involving backbone ^1H, ^{15}N, and ^{13}C and side-chain $^{13}C^{\beta}$ chemical shift difference data (Figures 4 and 5), coupled with the $\Delta^{13}C^{\alpha}$ data (Figure 9), indicate that the change in chemical and/or electronic environment throughout most of the mutant protein can be attributed to delocalized subtle structural perturbations and/or increased conformational flexibility rather than large-amplitude structural alterations.

Significance of a Cis Tyr92−Pro93 Peptide Bond in [C40A, C95A] RNase A. The fastest folding phase (U_{vf}) in disulfide-intact RNase A has been demonstrated to originate from unfolded species in which all four X−proline peptide groups are in their native isomerization states (Houry et al., 1994). This observation suggests that interactions involving local structures, which limit the conformational space of the unfolded protein, are responsible for these native X−proline states. Moreover, Dodge and Scheraga (1996) have presented data which suggest that strong, as yet undetermined, long-range interactions force a P93A RNase A mutant to adopt a native cis conformation, which is consistent with previous assertions that the type VI β-turn structure at Tyr92−Pro93 is sufficient for chain-folding initiation (Montelione et al., 1984; Oka et al., 1984; Montelione & Scheraga, 1989). An observed $^1H^{\alpha}_i-^1H^{\alpha}_{i+1}$ NOE between Tyr92 and Pro93, similar $^{13}C^{\beta}$ Pro93 chemical shifts for mutant and wild-type RNase A ($\Delta^{13}C^{\beta}_{wt-[C40A,C95A]} = 0.7$ ppm), statisti-

cal-coil $^{13}C^{\beta}$ values (Thanabal et al., 1994) for cis-proline ($|\Delta^{13}C^{\beta}_{\text{RNaseA}-\text{coil}}| < 0.5$ ppm), and significant chemical shift differences between statistical-coil $^{13}C^{\beta}$ values for cis and trans isomers of proline ($\Delta\delta = C^{\beta}_{\text{cis Pro coil}} - C^{\beta}_{\text{trans Pro coil}} =$ 2.6 ppm) collectively suggest that the Cys40−Cys95 cross-link does *not* stabilize this type VI β-turn structure in RNase A. Thus, the cis conformation of the X−Pro93 bond in [C40A, C95A] RNase A appears to be retained despite the greater conformational space accessible to the loop region encompassing this peptide bond arising from the removal of the Cys40−Cys95 disulfide cross-link.

Conformational and/or Dynamic Perturbation of Secondary Structures of [C40A, C95A] RNase A. Slowly exchanging amide proton resonances corresponding to Cys84 in β-sheet 1 and His105, Ala109, and His119 in β-sheet 2 of wild-type RNase A (Figure 10) were not observed in [C40A, C95A] RNase A at pH* 4.6 and 20 °C. All of these residues form backbone hydrogen bonds through their respective $^{1}H^{N}$ protons in the wild-type protein (Wlodawer, 1980). Moreover, statistically significant $^{1}H^{N}$ and ^{15}N chemical shift deviations from wild-type RNase A are observed for both Ala109 ($^{1}H^{N}$ $\Delta\delta = -0.19$, ^{15}N $\Delta\delta = 0.4$) and His119 ($^{1}H^{N}$ $\Delta\delta = 0.07$, ^{15}N $\Delta\delta = -1.1$). Similarly, the amide protons of Asn27, Gln28, Ser32, and Arg33 in α-helix 2 and Val43 in α-helix 3 are not observed in $^{1}H/^{2}H$ exchange experiments in the RNase A mutant. Care should be taken in interpreting these results because relative changes in local, subglobal, and global dynamic fluctuations in the folded structure (Hilton & Woodward, 1979; Englander & Kallenbach, 1984; Bai & Englander, 1996) of the mutant protein can increase the rate of exchange of backbone amide protons sufficiently to the point that they are "rapidly exchanging" (exchange rate constant > 0.02 s^{-1}). Following this reasoning, hydrogen-bonded structures in those residues of [C40A, C95A] RNase A where protection is no longer observed may be intact, albeit in rapid equilibrium. Accordingly, the complete disruption of the hydrogen bond between the Ala109 $^{1}H^{N}$ proton and the carboxyl oxygen of His119 is questionable since a $^{1}H^{N}-^{1}H^{N}$ NOE between these two residues is observed (Figure 10) in *both* the mutant and wild-type proteins, and there is no large ($|\Delta J| > 1.5$ Hz) difference in $3J(^{1}H^{N}-H^{\alpha})$. The $^{1}H^{N}-^{15}N$ correlation for Cys84 is weak in the 2D HSQC spectrum in $^{1}H_2O$ (Figure 3); consequently, no reliable conclusions can be drawn regarding disruption of the backbone hydrogen bonding for this residue in [C40A, C95A] RNase A.

Comparisons of short-range and medium-range NOE's and $^{3}J(^{1}H^{N}-H^{\alpha})$ coupling constants between wild-type and [C40A, C95A] RNase A indicate an overall similarity in the secondary structures of the two proteins. However, a significant number of interstrand NOE's within the β-sheet structures and characteristic $^{1}H^{N}_{i}-^{1}H^{\alpha}_{i-3}$ NOE's within the α-helical structures observed in the wild-type protein are absent from the corresponding mutant data. Moreover, significant differences were observed between the mutant and wild-type RNase A in the measured values of $^{3}J(^{1}H^{N}-H^{\alpha})$ coupling constants ($|\Delta J| > 1.5$ Hz) of residues located in the two β-sheets (Figure 10A, Asp83; Figure 10B, Val63, Ile107, and Val108) and in α-helix 1 (Ala6 and Arg10). Significantly, the absence of correlation within a specific region of the mutant protein between NOE's and protected amide protons, observed in the wild-type but not the mutant protein, and large deviations in $^{3}J(^{1}H^{N}-H^{\alpha})$ between the same two proteins also suggest that subtle delocalized differences in backbone conformation and/or conformational flexibility are responsible for these data.

Thermodynamic Contribution of the Cys40−Cys95 Disulfide Bond to RNase A Stability. A direct comparison of the enthalpies [$\Delta H°(T)$] and entropies [$\Delta S°(T)$] of unfolding between both of the [C40A, C95A] and [C40S, C95S] RNase A mutants and wild-type RNase A at the average transition temperature of the mutant proteins ($T_{\text{m [C40A,C95A],[C40S,C95S]}} \cong$ 33.65 °C; Table 1) indicates that the structures of both the *folded* and *unfolded* mutant proteins are affected. Values of 255 ± 18 cal/(mol deg) for the entropy of unfolding [$\Delta S°(T)$] and 84.7 ± 5.7 kcal/mol for the enthalpy [$\Delta H°(T)$] of unfolding (95% confidence) were determined for wild-type RNase A at 33.65 °C. These values were calculated by correcting the experimental values of $\Delta S°(T_m)$ and $\Delta H°(T_m)$ ($T_{\text{m wild-type}} = 55.5$ °C; Table 1) for wild-type RNase A, using the average value of the change in the heat capacity due to the denaturation of wild-type RNase A [$\Delta C_{p\ \text{wild-type}}(T) \cong 1.25$ kcal/(mol deg); Makhatadze & Privalov, 1995] over the temperature range from the transition temperature (T_m) of the wild-type protein (55.5 °C; Table 1) to the average transition temperature (T_m) of the [C40A, C95A] and [C40S, C95S] mutant proteins (33.65 °C; Table 1). The values for wild-type RNase A can be compared directly to the corresponding values of 238 ± 12 and 231 ± 6 cal/(mol deg) for the entropies of unfolding [$\Delta S°(T_m)$], and 72.9 ± 3.7 and 71.5 ± 1.8 kcal/mol for the enthalpies of unfolding [$\Delta H°(T_m)$], determined for the [C40A, C95A] ($T_{\text{m[C40A,C95A]}} = 33.7$ °C; Table 1) and [C40S, C95S] ($T_{\text{m[C40S,C95S]}} = 33.6$ °C; Table 1) mutants of RNase A, respectively.

It is generally understood that disruption of a disulfide cross-link destabilizes the native state relative to the denatured state because of the increased entropy of the denatured protein (Poland & Scheraga, 1965; Anfinsen & Scheraga, 1975; Lin et al., 1984; Pace et al., 1988; Doig & Williams, 1991; Cooper et al., 1992). If the native conformations of the mutant and wild-type proteins were the same, the mutant proteins lacking the Cys40−Cys95 disulfide cross-links would be expected to have *significantly larger* entropies of unfolding at 33.65 °C than the wild-type protein. Consequently, the *smaller* value of $\Delta S°(T)$ at 33.65 °C observed for both of the RNase A mutants indicates a more disordered folded state in the disulfide-deleted mutant proteins than in the native structure of wild-type RNase A. Similarly, the reduction in the $\Delta H°(T)$ observed in both [C40A, C95A] and [C40S, C95S] RNase A at 33.65 °C relative to the wild-type protein at the same temperature suggests that some structural alterations, such as disrupted hydrogen bonds or altered hydrophobic interactions, exist in the folded states of the mutant proteins. These alterations arise because disulfide bonds and noncovalent interactions mutually influence each other (Laskowski & Scheraga, 1954; Kuroki et al., 1992; Shimotakahara et al., 1997).

The relative thermodynamic stability of mutant and wild-type RNase A can be expressed quantitatively by the conformational chemical potential difference ($\Delta\mu°_{\text{conf}}$) between the native and denatured states of the respective proteins. Konishi et al. (1982b) first introduced $\Delta\mu°_{\text{conf}}$, which depends only on the conformation of the protein, to compare different folding intermediates of RNase A which differ only slightly in their chemical composition. Further-

more, Denton and Scheraga (1991) demonstrated that errors arising from the different heat capacities of the two proteins can be minimized if $\Delta\mu^\circ_{conf}$ is evaluated at a temperature midway between their respective T_m's. The conformational chemical potential differences between wild-type and both [C40A, C95A] and [C40S, C95S] RNase A [$\Delta\Delta\mu^\circ_{conf(transition)}$], evaluated at 44.6 °C, were identical (6.3 ± 0.3 kcal/mol). These values can be compared to the difference in free energies of the mutant and wild-type proteins in the *denatured* state arising from their different loop entropies (Lin et al., 1984). The values of the theoretical $\Delta\Delta\mu^\circ_{conf(loop)}$ between wild-type and both [C40A, C95A] and [C40S, C95S] RNase A, considering only the respective denatured states of the proteins, were also identical (4.71 kcal/mol). The difference between the theoretical and experimental values for the $\Delta\Delta\mu^\circ_{conf}$ was 1.6 kcal/mol for both mutants. This difference implies that substantial *destabilization of the native state* accompanies the deletion of the Cys40−Cys95 disulfide bond in RNase A. The accuracy of the theoretical values of the loop entropies relies on the approximation of applying a Gaussian distribution to short chains. Also, the value for $\Delta\Delta\mu^\circ_{conf(transition)}$ was calculated assuming the same values for the change in the heat capacity due to denaturation for [C40A, C95A] and [C40S, C95S] RNase A mutants as that which was determined for the wild-type protein [$\Delta C_{p[C40A,C95A]}(T)$ and $\Delta C_{p[C40S,\ C95S]}(T) \cong \Delta C_{p\ wild-type}(T)$ between $T = 33.6$ °C and 55.5 °C]. Although the experimental values of $\Delta C_{p[C40A,C95A]}(T)$ and $\Delta C_{p[C40S,C95S]}(T)$ were not determined explicitly, even a relatively large [±1 kcal/(mol deg)] change in $\Delta C_{p[C40A,C95A]}(T)$ or $\Delta C_{p[C40S,C95S]}(T)$ from the value observed for wild-type RNase A [$\Delta C_{p\ wild-type}(T) \cong 1.25$ kcal/(mol deg) between $T = 33.6$ and 55.5 °C] would account for only 0.3 kcal/mol of the 1.6 kcal/mol difference between the observed $\Delta\Delta\mu^\circ_{conf(transition)}$ and $\Delta\Delta\mu^\circ_{conf(loop)}$.

Relative Amide Exchange Rates between Wild-Type and [C40A, C95A] RNase A. Amide $^1H/^2H$ exchange rates can elucidate the nature of the dominant unfolding event occurring in rapid equilibrium at each observable residue of a protein (Linderstrøm-Lang, 1955; Hvidt & Nielsen, 1966; Englander & Kallenbach, 1984). Specifically, the exchange of amide protons is governed by the most highly populated local, subglobal, or global structural fluctuation that instantaneously disrupts hydrogen-bonded structures, thereby rendering the respective amide proton accessible to solvent exchange (Hilton & Woodward, 1979; Englander & Kallenbach, 1984; Bai & Englander, 1996). The ratio of backbone amide exchange rate constants between wild-type and [C40A, C95A] RNase A (Figures 7 and 8) clearly demonstrates a relatively uniform, large difference between the slowest exchanging amide protons in the respective proteins [$\log(k_{wild-type}/k_{[C40A,C95A]}) \sim 10^4-10^6$]. The large relative change in $^1H/^2H$ exchange rate constants between wild-type and [C40A, C95A] RNase A indicates significant global reductions in the conformational stability of the corresponding residues located primarily in the hydrophobic core of the mutant protein. The observation that some residues, such as those found in the N-terminal α-helix (α1) of wild-type RNase A, exhibit only moderate differences in $\log(k_{wild-type}/k_{[C40A,\ C95A]})$ can probably be attributed to local structural fluctuations in these residues as the dominant mechanism for amide proton exchange in both the mutant and wild-type protein. Such fluctuations occur considerably more frequently than global ones, even in the mutant protein, because of their lower activation energy (Englander & Kallenbach, 1984).

Comparison between Analogs of Des-[40−95] and Des-[65−72] Folding Intermediates. The oxidative regeneration pathways of RNase A, in the presence of oxidized and reduced DTT, proceed through two independent major and minor rate-determining three-disulfide species, des-[40−95] and des-[65−72], respectively (Rothwarf & Scheraga, 1991, 1993a−d; Rothwarf et al., 1995). Similarly, the reductive unfolding pathway of RNase A in the presence of reduced DTT also proceeds through the same two rate-determining intermediates (Li et al., 1995). The major and minor populated pathways in the reduction of RNase A are, however, the reverse of the regeneration pathways, with the major and minor rate-determining three-disulfide species being des-[65−72] and des-[40−95], respectively (Li et al., 1995).

From the structural and conformational characterization of an analog of des-[40−95] presented here and two parallel studies of blocked and mutant analogs of des-[65−72] (Talluri et al., 1994; Shimotakahara et al., 1997), direct comparisons of these two intermediates in terms of their respective roles in the folding and unfolding of RNase A can now be made. Both intermediate analogs of des-[65−72] and des-[40−95] are globally destabilized relative to the wild-type protein throughout their native structures as indicated by their lower T_m's and overall faster $^1H/^2H$ amide exchange rates. The *relative* stabilities of the two analogs of des-[40−95] and des-[65−72], however, are not equal. The des-[40−95] analog exhibits considerably lower thermal stability ($\Delta T_{m[C65S,C72S]-[C40S,C95S]} = 4.6$ °C) and more pronounced delocalized conformational perturbations and/or increased conformational dynamics than the des-[65−72] analogs as indicated from $^1H/^2H$ amide proton exchange rates, $^3J(^1H^N-^1H^\alpha)$ values, and NOE data. It should be noted that a lower thermodynamic stability of the des-[40−95] analog, [C40A, C95A] RNase A, is expected since the denatured state for this analog of des-[40−95] has more entropy than the denatured state of the des-[65−72] analog, [C65S, C72S] RNase A (value of $\Delta\Delta\mu^\circ_{conf(loop)\{[C40A,C95A]-[C65S,C72S]\}} = 0.8$ kcal/mol, considering only differences in loop entropies of the denatured states). Moreover, comparison of the measured values of $\Delta\Delta\mu^\circ_{conf}$ from reversible thermal unfolding curves ($\Delta\Delta\mu^\circ_{conf(transition)\{[C40A,C95A]-[C65S,C72S]\}} = 1.1$ kcal/mol), which reflect differences in entropies of both the *folded* and *unfolded* states of the des-[40−95] and des-[65−72] analogs, suggests that the entropies of the folded states of the two analogs are similar ($\Delta\Delta\mu^\circ_{conf(loop)} - \Delta\Delta\mu^\circ_{conf(transition)} \cong 0.3$ kcal/mol).

Although analogs of both des-[40−95] ([C40A, C95A] RNase A) and des-[65−72] ([C65S, C72S] RNase A) (Shimotakahara et al., 1997) exhibit significant destabilization of the hydrophobic core relative to the wild-type protein, the regions of local structural perturbation in the two analogs are *different*. Specifically, the structural characterization of [C40A, C95A] RNase A indicates that disruption of the Cys40−Cys95 disulfide bond in des-[40−95] does not facilitate the breakage of the Cys65−Cys72 disulfide bond through structural perturbation. In fact, the region encompassing Cys65−Cys72 in [C40A, C95A] RNase A is the most native-like region in the protein (see, for example, Figure 5). This observation is in agreement with the

regeneration and reduction studies which indicate that the two pathways for both regeneration and reduction involve conformationally distinct transition states (Li et al., 1995).

Significant advances were made in understanding the complex mechanism of oxidative regeneration of RNase A when the major rate-determining intermediates were identified (Rothwarf & Scheraga, 1991, 1993a−d; Rothwarf et al., 1995). Structural characterizations of analogs of both the major ([C40A, C95A] RNase A, presented here) and minor ([C65S, C72S] RNase A; Shimotakahara et al., 1977) rate-determining intermediates, des-[40−95] and des-[65−72], provide greater insight into the nature of these precursors and their relationships to the native protein structure in the oxidative regeneration of wild-type RNase A.

ACKNOWLEDGMENT

We thank M. A. McDonald for cloning the DNA vectors pRM[C40A, C95A], T. W. Thanhauser and D. M. Rothwarf for experimental assistance and many helpful discussions, R. T. Raines for providing us with the DNA expression vector pXBR-2, and Molecular Simulations Inc. for providing us with the program FELIX.

SUPPORTING INFORMATION AVAILABLE

Table S1, ^{1}H, ^{15}N, and ^{13}C backbone and $^{13}C^{\beta}$ side-chain assignments for [C40A, C95A] RNase A; Table S2, $^{3}J(H^{N}-H^{\alpha})$ values (Hz) for wild-type and [C40A, C95A] RNase A at pH 4.6 and 20 °C; and Table S3, ^{1}H side-chain assignments for [C40A, C95A] RNase A (14 pages). Ordering information is given on any current masthead page.

REFERENCES

Ahmed, A. K., Schaffer, S. W., & Wetlaufer, D. B. (1975) *J. Biol. Chem. 250*, 8477−8482.
Altmann, K.-H., & Scheraga, H. A. (1990) *J. Am. Chem. Soc. 112*, 4926−4931.
Anfinsen, C. B. (1973) *Science 181*, 223−230.
Anfinsen, C. B., & Scheraga, H. A. (1975) *Adv. Protein Chem. 29*, 205−300.
Bai, Y., & Englander, S. W. (1996) *Proteins 24*, 145−151.
Bax, A., & Davis, D. G. (1985) *J. Magn. Reson. 65*, 355−360.
Bax, A., & Grzesiek, S. (1993) *Acc. Chem. Res. 26*, 131−138.
Boucher, W., Laue, E. D., Campbell-Burk, S. L., & Domaille, P. J. (1992) *J. Biomol. NMR 2*, 631−637.
Braunschweiler, L., & Ernst, R. R. (1983) *J. Magn. Reson. 53*, 521−528.
Buckler, D. R., Haas, E., & Scheraga, H. A. (1995) *Biochemistry 34*, 15965−15978.
Chazin, W. J., Kördel, J., Drakenberg, T., Thulin, E., Brodin, P., Grundström, T., & Forsén, S. (1989) *Proc. Natl. Acad. Sci. U.S.A. 86*, 2195−2198.
Clore, G. M., & Gronenborn, A. M. (1991) *Prog. NMR Spectrosc. 23*, 43−92.
Clubb, R. T., Thanabal, V., & Wagner, G. (1992) *J. Magn. Reson. 97*, 213 −217.
Cooper, A., Eyles, S. J., Radford, S. E., & Dobson, C. M. (1992) *J. Mol. Biol. 225*, 939−943.
Creighton, T. E. (1974) *J. Mol. Biol. 87*, 563−577.
Creighton, T. E. (1977a) *J. Mol. Biol. 113*, 275−293.
Creighton, T. E. (1977b) *J. Mol. Biol. 113*, 329−341.
Creighton, T. E. (1988) *Bioessays 8*, 57−63.
Creighton, T. E., & Goldenberg, D. P. (1984) *J. Mol. Biol. 179*, 497−526.
Crook, E. M., Mathias, A. P., & Rabin, B. R. (1960) *Biochem. J. 74*, 234−238.
Dadlez, M., & Kim, P. S. (1996) *Biochemistry 35*, 16153−16164.
Darby, N. J., van Mierlo, C. P. M., Scott, G. H. E., Neuhaus, D., & Creighton, T. E. (1992) *J. Mol. Biol. 224*, 905−911.
delCardayré, S. B., Ribó, M., Yokel, E. M., Quirk, D. J., Rutter, W. J., & Raines, R. T. (1995) *Protein Eng. 8*, 261−273.
Denton, M. E., & Scheraga, H. A. (1991) *J. Protein Chem. 10*, 213−232.
Dodge, R. W., & Scheraga, H. A. (1996) *Biochemistry 35*, 1548−1559.
Doig, A. J., & Williams, D. H. (1991) *J. Mol. Biol. 217*, 389−398.
Englander, S. W., & Kallenbach, N. R. (1984) *Q. Rev. Biophys. 16*, 521−655.
Evans, P. A., Dobson, C. M., Kautz, R. A., Hatfull, G., & Fox, R. O. (1989) *Nature 329*, 266−268.
Feng, W., Rios, C. B., & Montelione, G. T. (1996) *J. Biomol. NMR 8*, 98−104.
Freund, S. M. V., Wong, K.-B., & Fersht, A. R. (1996) *Proc. Natl. Acad. Sci. U.S.A. 93*, 10600−10603.
Goldenberg, D. P. (1992) *Trends Biochem. Sci. 17*, 257−261.
Grzesiek, S., & Bax, A. (1992a) *J. Am. Chem. Soc. 114*, 6291−6293.
Grzesiek, S., & Bax, A. (1992b) *J. Magn. Reson. 99*, 201−207.
Hantgen, R. R., Hammes, G. G., & Scheraga, H. A. (1974) *Biochemistry 13*, 3421−3431.
Hermans, J., Jr., & Scheraga, H. A. (1961) *J. Am. Chem. Soc. 83*, 3283−3292.
Hilton, B. D., & Woodward, C. K. (1979) *Biochemistry 18*, 5834−5841.
Houry, W. A., Rothwarf, D. M., & Scheraga, H. A. (1994) *Biochemistry 33*, 2516−2530.
Hurd, R. E., & John, B. K. (1991) *J. Magn. Reson. 91*, 648−653.
Hurle, M. R., Eads, C. D., Pearlman, D. A., Seibel, G. L., Thomason, J., Kosen, P. A., Kollman, P., Anderson, S., & Kuntz, I. D. (1992) *Protein Sci. 1*, 91−106.
Hvidt, A., & Nielsen, S. O. (1966) *Adv. Protein Chem. 21*, 287−386.
Jansson, M., Li, Y. C., Jendeberg, L., Anderson, S., Montelione, G. T., & Nilsson, B. (1996) *J. Biomol. NMR 7*, 131−141.
Jeener, J., Meier, B. H., Bachmann, P., & Ernst, R. R. (1979) *J. Chem. Phys. 71*, 4546−4553.
Kay, L. E. (1995) *Prog. Biophys. Mol. Biol. 63*, 277−299.
Kay, L. E., Keifer, P., & Saarinen, T. (1992) *J. Am. Chem. Soc. 114*, 10663−10665.
Kim, P. S., & Baldwin, R. L. (1990) *Annu. Rev. Biochem. 59*, 631−660.
Konishi, Y., Ooi, T., & Scheraga, H. A. (1981) *Biochemistry 20*, 3945−3955.
Konishi, Y., Ooi, T., & Scheraga, H. A. (1982a) *Biochemistry 21*, 4734 −4740.
Konishi, Y., Ooi, T., & Scheraga, H. A. (1982b) *Biochemistry 21*, 4741−4748.
Konishi, Y., Ooi, T., & Scheraga, H. A. (1982c) *Proc. Natl. Acad. Sci. U.S.A. 79*, 5734−5738.
Kuboniwa, H., Grzesiek, S., Delaglio, F., & Bax, A. (1994) *J. Biomol. NMR 4*, 871−878.
Kumar, A., Ernst, R. R., & Wüthrich, K. (1980) *Biochem. Biophys. Res. Commun. 95*, 1−6.
Kuroki, R., Inaka, K., Taniyama, Y., Kidokoro, S., Matsushima, M., Kikuchi, M., & Yutani, K. (1992) *Biochemistry 31*, 8323−8328.
Laity, J. H., Shimotakahara, S., & Scheraga, H. A. (1993) *Proc. Natl. Acad. Sci. U.S.A. 90*, 615−619.
Laskowski, M., Jr., & Scheraga, H. A. (1954) *J. Am. Chem. Soc. 76*, 6305−6319.
Li, Y.-J., Rothwarf, D. M., & Scheraga, H. A. (1995) *Nat. Struct. Biol. 2*, 489 −494.
Lin, S. H., Konishi, Y., Denton, M. E., & Scheraga, H. A. (1984) *Biochemistry 23*, 5504−5512.
Linderstrøm-Lang, K. (1955) *Chem. Soc., Spec. Publ. 2*, 1−20.
Macura, S., & Ernst, R. R. (1980) *Mol. Phys. 41*, 95−117.
Makhatadze, G. I., & Privalov, P. L. (1995) *Adv. Protein Chem. 47*, 307−425.
Marion, D., Ikura, M., Tschudin, R., & Bax, A. (1989) *J. Magn. Reson. 85*, 393−399.
Matheson, R. R., & Scheraga, H. A. (1978) *Macromolecules 11*, 819−829.
Montelione, G. T., & Scheraga, H. A. (1989) *Acc. Chem. Res. 22*, 70−76.

Montelione, G. T., & Wagner, G. (1989) *J. Am. Chem. Soc. 111*, 5474−5475.
Montelione, G. T., Arnold, E., Meinwald, Y. C., Stimson, E. R., Denton, J. B., Huang, S.-G., Clardy, J., & Scheraga, H. A. (1984) *J. Am. Chem. Soc. 106*, 7946−7958.
Moy, F. J., Seddon, A. P., Campbell, E. B., Böhlen, P., & Powers, R. (1995) *J. Biomol. NMR 6*, 245−254.
Muhandiram, D. R., & Kay, L. E. (1994) *J. Magn. Reson., Ser. B 103*, 203−216.
Naderi, H. M., Thomason, J. F., Borgias, B. A., Anderson, S., James, T. L., & Kuntz, I. D. (1991) in *Conformations and Forces in Protein Folding* (Nall, B. T., & Dill, K. A., Eds.) pp 86−114, American Association for the Advancement of Science, Washington, DC.
Nagayama, K. (1986) *J. Magn. Reson. 69*, 508−510.
Némethy, G., & Scheraga, H. A. (1979) *Proc. Natl. Acad. Sci. U.S.A. 76*, 6050−6054.
Oka, M., Montelione, G. T., & Scheraga, H. A. (1984) *J. Am. Chem. Soc. 106*, 7959−7969.
Pace, C. N., Grimsley, G. R., Thomson, J. A., & Barnett, B. J. (1988) *J. Biol. Chem. 263*, 11820−11825.
Palmer, A. G., III, Williams, J., & McDermott, A. (1996) *J. Phys. Chem. 100*, 13293−13310.
Pardi, A., Billeter, M., & Wüthrich, K. (1984) *J. Mol. Biol. 180*, 741−751.
Poland, D. C., & Scheraga, H. A. (1965) *Biopolymers 3*, 379−399.
Privalov, P. L., Tiktopulo, E. I., & Khechinashvili, N. N. (1973) *Int. J. Pept. Protein Res. 5*, 229−237.
Richardson, J. S. (1981) *Adv. Protein Chem. 34*, 167−339.
Rico, M., Bruix, M., Santoro, J., Gonzalez, C., Neira, J. L., Nieto, J. L., & Herranz, J. (1989) *Eur. J. Biochem. 183*, 623 −638.
Rios, C. B., Feng, W., Tashiro, M., Shang, Z., & Montelione, G. T. (1996) *J. Biomol. NMR 8*, 345−350.
Robertson, A. D., Purisma, E. O., Eastman, M. A., & Scheraga, H. A. (1989) *Biochemistry 28*, 5930−5938.
Rothwarf, D. M., & Scheraga, H. A. (1991) *J. Am. Chem. Soc. 113*, 6293−6294.
Rothwarf, D. M., & Scheraga, H. A. (1993a) *Biochemistry 32*, 2671−2679.
Rothwarf, D. M., & Scheraga, H. A. (1993b) *Biochemistry 32*, 2680−2689.
Rothwarf, D. M., & Scheraga, H. A. (1993c) *Biochemistry 32*, 2690−2697.
Rothwarf, D. M., & Scheraga, H. A. (1993d) *Biochemistry 32*, 2698−2703.
Rothwarf, D. M., Li, Y. -J., & Scheraga, H. A. (1995) *Protein Sci. 4* (Suppl. 2), 237S.
Santoro, J., Gonzalez, C., Bruix, M., Neira, J. L., Nieto, J. L., Herranz, J., & Rico, M. (1993) *J. Mol. Biol. 229*, 722−734.
Scheraga, H. A., Konishi, Y., Rothwarf, D. M., & Mui, P. W. (1987) *Proc. Natl. Acad. Sci. U.S.A. 84*, 5740−5744.
Shimotakahara, S., Rios, C. B., Laity, J. H., Zimmerman, D. E., Scheraga, H. A., & Montelione, G. T. (1997) *Biochemistry 36*, 6915−6929.
Spera, S., & Bax, A. (1991) *J. Am. Chem. Soc. 113*, 5490−5492.
Staley, J. P., & Kim, P. S. (1992) *Proc. Natl. Acad. Sci. U.S.A. 89*, 1519 −1523.
Talluri, S., Montelione, G. T., van Duyne, G., Piela, L., Clardy, J., & Scheraga, H. A. (1987) *J. Am. Chem. Soc. 109*, 4473−4477.
Talluri, S., Rothwarf, D. M., & Scheraga, H. A. (1994) *Biochemisrtry 33*, 10437−10449.
Thanabal, V., Omecinsky, D. O., Reily, M. D., & Cody, W. L. (1994) *J. Biomol. NMR 4*, 47−59.
Thannhauser, T. W., & Scheraga, H. A. (1985) *Biochemistry 24*, 7681 −7688.
Thornton, J. M. (1981) *J. Mol. Biol. 151*, 261−287.
Tsong, T. Y., Hearn, R. P., Wrathall, D. P., & Sturtevant, J. M. (1970) *Biochemistry 9*, 2666−2677.
Udgaonkar, J. B., & Baldwin, R. L. (1990) *Proc. Natl. Acad. Sci. U.S.A. 87*, 8197−8201.
van Mierlo, C. P. M., Darby, N. J., Neuhaus, D., & Creighton, T. E. (1991) *J. Mol. Biol. 222*, 353−371.
van Mierlo, C. P. M., Darby, N. J., Keeler, J., Neuhaus, D., & Creighton, T. E. (1993) *J. Mol. Biol. 229*, 1125−1146.
Vuister, G. W., & Bax, A. (1993) *J. Am. Chem. Soc. 115*, 7772−7777.
Wearne, S. J., & Creighton, T. E. (1988) *Proteins 4*, 251−261.
Weissman, J. S., & Kim, P. S. (1991) *Science 253*, 1386−1393.
Weissman, J. S., & Kim, P. S. (1992a) *Proc. Natl. Acad. Sci. U.S.A. 89*, 9900−9904.
Weissman, J. S., & Kim, P. S. (1992b) *Cell 71*, 841−851.
Weissman, J. S., & Kim, P. S. (1993) *Nature 365*, 185−188.
Weissman, J. S., & Kim, P. S. (1995) *Nat. Struct. Biol. 2*, 1123−1130.
Wishart, D. S., Bigam, C. G., Yao, J., Abildgaard, F., Dyson, H. J., Oldfield, E., Markley, J. L., & Sykes, B. D. (1995) *J. Biomol. NMR 6*, 135−140.
Wlodawer, A. (1980) *Acta Crystallogr. B36*, 1826−1831.
Wlodawer, A., Svensson, L. A., Sjölin, L., & Gilliland, G. L. (1988) *Biochemistry 27*, 2705−2717.
Wright, P. E., Dyson, H. J., & Lerner, R. A. (1988) *Biochemistry* 27, 7167−7175.
Wüthrich, K. (1989) *Science 243*, 45−50.
Xu, X., Rothwarf, D. M., & Scheraga, H. A. (1996) *Biochemistry 35*, 6406−6417.
Zhu, G., & Bax, A. (1990) *J. Magn. Reson. 90*, 405−410.
Zimmerman, D. E., & Montelione, G. T. (1995) *Curr. Opin. Struct. Biol. 5*, 664−673.
Zimmerman, D., Kulikowski, C. A., Wang, L., Lyons, B., & Montelione, G. T. (1994) *J. Biomol. NMR 4*, 241−256.
Zimmerman, D. E., Kulikowski, C. A., Huang, Y., Feng, W., Tashiro, M., Chien, C.-Y., Powers, R., & Montelione, G. T. (1997) *J. Mol. Biol.* (in press).
Zuiderweg, E. R. P., & Fesik, S. W. (1989) *Biochemistry 28*, 2387−2391.

BI970878B